Supplemental Material

CADHERIN-11 BLOCKADE REDUCES INFLAMMATION-DRIVEN FIBROTIC REMODELING AND IMPROVES OUTCOMES AFTER MYOCARDIAL INFARCTION

Schroer, Cadherin-11 regulates fibrotic remodeling after MI

Alison K. Schroer, PhD[a], Matthew R. Bersi, PhD[a], Cynthia R. Clark, PhD[a], Qinkun Zhang, MD[b], Lehanna H. Sanders, PhD[b], Antonis K. Hatzopoulos, PhD[b], Thomas L. Force, MD[b], Susan M. Majka, PhD[c], Hind Lal, PhD[b], and W. David Merryman, PhD[a]

[a] Department of Biomedical Engineering, [b] Department of Cardiovascular Medicine, [c] Department of Allergy, Pulmonary, and Critical Care Medicine, Vanderbilt University, Nashville, TN, USA 37253

For Correspondence:
W. David Merryman
Room 9445D MRB4
2213 Garland Ave
Nashville, TN 37212
P: 615.322.7219
F: 615.322.6541
E: david.merryman@vanderbilt.edu

Detailed Methods

Mice

All animal procedures were approved by the Institutional Animal Care and Use Committee at Vanderbilt University. Myocardial infarction (MI) was induced by permanent ligation of the left anterior descending (LAD) coronary artery, as previously described (Gao et al. 2010). Briefly, mice were anesthetized by 2% isoflurane inhalation, without ventilation, and a small skin incision was made over the left chest. After dissection and retraction of the pectoral major and minor muscles, the 4th intercostal space was exposed and a small hole was made to open the pleural membrane and pericardium. The heart was then gently popped out through the hole and the LAD was ligated ~3 mm from its origin using a 6-0 silk suture. Successful ligation was confirmed by pale coloration of the anterior wall of the left ventricle. Following LAD ligation, the heart was placed back into the intra-thoracic space, air was evacuated from the thoracic cavity, and the muscle and skin was sutured closed. MI was performed in 12 to 16 week old male *Cadherin-11* deficient mice (*Cdh11*$^{+/+}$, *Cdh11*$^{+/-}$, *Cdh11*$^{-/-}$) or WT male mice (C57BL/6J; Jackson Laboratories). All mice were given pre- and post-operative analgesic of 5 mg/kg ketoprofen every 24 hours for 72 hours.

For antibody treatments, mice were administered either 10 mg/kg of a cadherin-11 (CDH11) functional blocking antibody (SYN0012; with permission from Roche) or an isotype control antibody (IgG2a) resuspended in sterile saline. Antibodies were delivered by intraperitoneal (IP) injection every four days, beginning one day after surgery, with the last treatment given on day 17 after infarct. Comparisons between survival curves were evaluated using the Gehan-Breslow-Wilcoxon test.

Isolation of cardiomyocyte and non-cardiomyocyte cells

Live cardiac cells were isolated from mouse hearts as previously described (O'Connell, Rodrigo, and Simpson 2007). Briefly, slow perfusion of the heart with a collagenase solution was used to digest the ECM and isolate intact cardiomyocytes (CMs) and non-CMs from hearts. Cells were separated into CM and non-CM fractions by centrifugation for 10 min at 90 g and lysed in TRIZOL for analysis of *Cdh11* transcription. Transcription of *Cdh11* in both cell types was normalized to CM expression and compared with a Student's t-test.

Identification of non-CM cell types by flow cytometry

Composition of cell types in the heart and the peripheral blood were measured by flow cytometry. Hearts were isolated at either three or seven days after Sham or MI surgery and immediately placed in a solution of ice cold FACS buffer (5% FBS in PBS). The atria were removed and the ventricular tissue was minced and stored on ice. Minced samples were placed in 2 mL of digestion solution, comprised of 1.4 mg/mL of type II collagenase in HBSS, and incubated at 37°C for thirty minutes with rotation. The digested sample was then triturated forcefully and filtered through a 100 μm cell strainer. Resultant cells were washed in 50 mL of ice cold FACS buffer, centrifuged at 1500 rpm for 5 minutes, resuspended in FACS buffer and filtered through a 70 μm cell strainer into room temperature red blood cell lysis buffer (BioLegend). Similarly, peripheral blood was collected with a K-EDTA syringe by cardiac puncture and quickly diluted into room temperature red blood cell lysis buffer. After 5 minutes in lysis buffer, cells were washed in FACS buffer, centrifuged at 1500 rpm for 5 minutes, and counted to measure the total number of cells. Cells were then taken from each sample, suspended in DAPI (1:100,000; Thermo-Fisher Scientific) to label dead cells, and stained with conjugated antibodies for Ter-119 (1:100; violetFluor™ 450 clone TER-119; Tonbo Biosciences), CD45.2 (1:100; PerCP-Cy5.5 clone 104; Tonbo Biosciences),

CD31 (1:100; PE-Cy7 clone MEC13.3; BioLegend), CD11b (1:100; PE clone M1/70; eBioscience), CD206 (1:100; APC clone MR6F3; eBioscience), CD86 (1:100; FITC clone GL1; eBioscience), Gr-1 (1:100; FITC clone RB6-8C5; eBioscience). Staining for CDH11 was performed in a two-step process with an unconjugated primary antibody (1:100; clone 23C6; from M. Brenner (Chang et al. 2017)) followed by a PE secondary antibody (1:100; PE clone; RMG1-1; BioLegend). Note that antibodies specific for CD45.1 (1:100; PE clone A20; BD Biosciences) and CD45.2 (1:100; FITC clone 104; BD Biosciences) were used for assessment of bone marrow engraftment efficiency (**Figure S6**).

Gating based on size and shape (FSC and SSC), in addition to negative staining for DAPI and Ter-119, was used to identify viable single cells (**Figure S1**). Further gating based on fluorescence minus one (FMO) stained controls was used to identify the presence of distinct cell populations (**Figure S2**). In particular, we identified bone marrow derived cells (BMDC: $CD45^{+}$), cardiac endothelial cells (CEC: $CD45^{-}CD11b^{-}CD31^{+}$), and cardiac mesenchymal cells – primarily myofibroblasts – (CMC: $CD45^{-}CD11b^{-}CD31^{-}$). Within the BMDC population, we gated for bone marrow-derived pro-angiogenic cells (BMD-PACs: $CD45^{+}CD11b^{-}CD31^{+}$), myeloid lineage cells ($CD45^{+}CD11b^{+}$), and non-myeloid lineage cells ($CD45^{+}CD11b^{-}CD31^{-}$). Note that non-myeloid lineage cells are predominately lymphocytes. Within the myeloid cell population, we identified various subpopulations including neutrophils ($CD45^{+}CD11b^{+}$Gr-$1/CD86^{hi}$), eosinophils ($CD45^{+}CD11b^{+}$Gr-$1/CD86^{lo}SSC^{hi}$), monocytes ($CD45^{+}CD11b^{+}$Gr-$1/CD86^{lo}SSC^{lo}$), and macrophages ($CD45^{+}CD11b^{+}$Gr-$1/CD86^{int}$) (Rose, Misharin, and Perlman 2012). Using this strategy, we further assessed macrophage polarization by gating for pro-inflammatory (M1-like) macrophages ($CD45^{+}CD11b^{+}$Gr-$1/CD86^{int}CD206^{-}$) and pro-resolving (M2-like) macrophages ($CD45^{+}CD11b^{+}$Gr-$1/CD86^{int}CD206^{+}$) (**Figure S1**). The neutrophil-to-lymphocyte ratio (NLR) was computed by dividing the number of positively identified neutrophils by the number of non-myeloid BMDCs in each sample (Chen et al. 2018).

Using the FMO control for CDH11 (**Figure S2**), this overall gating strategy was applied to 1) all live, single cells and 2) all live, $CDH11^{+}$ cells (**Figure S4C-D**). In this manner, we were able to compute the fraction of $CDH11^{+}$ cells within each cell population of interest identified in the heart (**Figure S3A** and **Figure 1**) and peripheral blood (**Figure S3B** and **FigureS5**). For studies involving SYN0012 and IgG2a treatments (**Figure 5** and **Figure S13**), the same gating strategy was used to identify cell populations of interest, although staining for CDH11 expression was not performed. Two-way ANOVA with Holms-Sidak's multiple comparison tests were used to determine significant changes in cell fraction between treatment groups and between days. The non-parametric Kruskal-Wallis test was used when the data being compared failed normality and equal variance tests.

Quantification of cardiac function and geometry by echocardiography

Ejection fraction (EF), left ventricular (LV) mass, and LV volume in both systole and diastole were measured from short axis cardiac M-Mode images captured on a Vevo 2100 small animal ultrasound system (VisualSonics). A minimum of six independent measures of LV diameter and wall thickness were used to calculate metrics of cardiac function and geometry for each mouse at each time point. Note that EF, LV mass and LV volume were calculated from the LV inner diameter at diastole and systole.

Echocardiographic measurements were made just prior to MI (baseline), as well as at days seven, 21, and 56 days after surgery. Mice with an EF reduced by less than 5% or greater than 70% were excluded from subsequent analyses. This ensured that all mice included in the study had consistently-sized (intermediate to large) infarcts which had not progressed to complete heart failure. In particular, for each group within the antibody treatment experiment, one mouse was excluded for a minor infarct and two were excluded with too large of an infarct. LV Mass measurements greater than 450 mg were excluded as outliers, likely caused by image artifacts due to fibrotic remodeling (only observed in

genotype comparison). Mice were euthanized by CO_2 inhalation in accordance with university guidelines at three, seven, 21 and 56 days after infarct for further processing.

Linear mixed-effect statistical analysis with the restricted maximum likelihood (REML) was performed to compare repeated measurements of echocardiological measurements in the same animals across times, treatments and genotypes. We considered the fixed effects (type III) for overall significant differences due to line/treatment group, day, and interaction between line and day. The post-hoc Holm-Sidak's method with an overall significance level of 0.05 was used to correct for multiple comparisons between days within a treatment group or genotype and to compare the effect of treatment within each day.

Bone marrow transplantation

Six week old male WT mice expressing the CD45.1 allele (B6.SJL-*Ptprc*^{a}*Pepc*^{b}/BoyJ; Jackson Laboratories) were lethally irradiated with a 10 Gy split dose from a Cs^{137} source (5 Gy in the morning followed by 5 Gy 4-6 hours later). Within 24 hours, age- and gender-matched *Cdh11*$^{+/+}$, *Cdh11*$^{+/-}$, and *Cdh11*$^{-/-}$ donors were euthanized and bone marrow was isolated from whole femurs and tibia. Donor bone marrow was delivered to irradiated recipients by retro-orbital injection (1×10^{6} cells in 100µL), and recipient mice were maintained on acidified water with antibiotics (neomycin and polymyxin B) for up to 2 weeks. Transplant efficiency was confirmed by flow cytometric analysis of isolated bone marrow showing simultaneous expression of the donor CD45.2 allele and absence of the original CD45.1 allele (**Figure S6**). To allow sufficient time for bone marrow reconstitution, mice received MI by permanent LAD ligation six weeks after transplantation.

Cryosectioning and quantitative histological analysis

Following euthanasia, hearts were dissected into PBS, weighed (**Figure S10A-B**), and then submerged briefly in a KCl solution to relax the CMs. Relaxed hearts were then bisected along the transverse plane (orthogonal to the long axis of the heart), embedded in OCT media, and frozen. Frozen blocks were subsequently cryosectioned into 10 μm sections, mounted onto glass slides, and stored at –20°C. A selection of the slides were stained using Masson's trichrome (Sigma), according to the manufacturer's instructions, in order to identify regions of healthy myocardium (red/pink), collagen/ECM deposition (blue), and cell nuclei (black) (**Figure S9**). Prior to staining, slides were brought to room temperature, OCT media was dissolved in PBS, and sections were fixed in Bouin's solution.

To quantify infarct morphology (length and thickness) from Masson's trichrome stained sections, a semi-automated image processing pipeline was developed (**Figure S9**). Briefly, non-uniformity in background illumination was corrected by bottom hat filtering prior to boundary detection. Using the detected boundaries, local ventricular wall thickness was computed using an Eulerian solution to a pair of linear partial differential equations over the histological domain (Yezzi and Prince 2003). By solving the Laplace equation for a given harmonic function f between the inner (ventricular lumen) and outer (myocardial wall) boundaries, the local thickness field was obtained. Correspondence trajectories along f between the inner and outer boundaries were used to subdivide histological sections into 40 circumferential partitions. (Rocha, Yezzi, and Prince 2007). Following partitioning, colorimetric segmentation in an HSL color space (Bersi et al. 2017) was performed in order to identify the area fractions of myocardium (red; H = 250° - 25°, S = 0.1 - 1.0, L = 0.1 - 0.93) and collagen (blue; H = 150° - 250°, S = 0.1 - 1.0, L = 0.1 - 0.93) within each partition. Based on the identified area fractions, locations of infarct borders were defined based on the inversion of area fractions (i.e., clockwise from red > blue to blue > red and vice-versa). Using this approach, the location and thickness profile of the infarcted regions were automatically identified. In cases of poor automatic detection, infarct borders were defined

manually. Finally, following identification of infarct borders, the ratio of infarct length to total circumferential length (in degrees) was used to estimate the percent circumference of the infarct region. Using the thickness profile between infarct borders, the average and standard deviation (i.e., thickness variation) were used to characterize infarct morphology (**Figure S10D-E**). Quantification was performed on 3 sections per heart separated by at least 300 μm.

Immunohistochemistry

Frozen slides were brought to room temperature, OCT media was dissolved in PBS, and tissue sections were fixed in 4% paraformaldehyde with 0.3% Triton-X for 10 min followed by blocking in 1% BSA in PBS for 1 hour. Tissue sections were then stained for either αSMA (Cy3; Sigma), CD31 (Biolegend: Alexa Fluor 594, clone 390), CD45 (FITC CD45.1; BD Pharmigen) or IL-6 (Abcam: clone 1A4). Sections stained with non-conjugated antibodies (IL-6) were incubated at a 1:100 dilution in 1% BSA overnight at 4°C. Sections were then rinsed with PBS and incubated with fluorescently tagged secondary antibodies (Goat anti Rabbit Alexa Fluor 647, Thermo) for 1 hour at a 1:300 dilution in 1% BSA. Sections stained with directly conjugated antibodies were incubated at a 1:100 dilution in 1% BSA for 1 hour at room temperature. Stained slides were mounted in ProLong Gold with DAPI to visualize cell nuclei and were imaged using an Olympus BX53 microscope equipped with a high resolution Qimaging Retiga 3000 camera. Muscularized vessels smaller than ~100 μm in diameter and myofibroblasts (defined as αSMA positive cells not colocalized with endothelial cells) present in one transverse section per heart collected from the center of the infarct zone were manually counted. The average number of muscularized vessels and myofibroblasts from hearts 21 days post-MI were compared with a Student's t-test.

Atomic force microscopy

Frozen slides were acclimated to room temperature, OCT media was dissolved in PBS, and tissue sections were blocked in 10% FBS for 20 minutes. Tissue sections were then stained for αSMA (Sigma) and a Hoechst nuclear stain (Invitrogen) for 20 minutes to allow for visualization of the infarct while scanning with the atomic force microscope (AFM). The Biocatalyst AFM developed by Bruker was used to measure tissue topography and stiffness within SYN0012 and IgG2a treated infarcts. The AFM probe was equipped with a blunted pyramidal tip specifically developed for soft biological samples (MLCT-Bio) and the peak force quantitative nanomechanical mapping scanning mode (PeakForce QNM) was used in order to provide robust measurements of topography and elastic modulus. Prior to scanning tissue samples, the system was calibrated on 40 kPa polyacrylamide gel standards and the spring constant and deflection sensitivity of the AFM probe was calculated. All measurements were made in PBS and were acquired from at least five separate 10x10 μm^2 areas from a minimum of two different sections per mouse (**Figure S8**). The median and interquartile range of stiffness from each scan were averaged for each mouse, and these measurements were averaged and compared by two-way ANOVA. The post-hoc Holm-Sidak's method with an overall significance level of 0.05 was used to account for multiple comparisons between treatment groups and different days.

Cell isolation and culture

To complement and inform our *in vivo* studies, cardiac fibroblasts (CFs) (Golden et al. 2012) and intraperitoneal macrophages (MΦs) were isolated from mice. CFs were isolated from *Cdh11*$^{+/+}$ and *Cdh11*$^{-/-}$ mice bred onto the *Immorto* mouse line, such that cells from littermate controls could be maintained in culture for longer. Briefly, hearts from eight week old mice were isolated, minced, and digested in a 2% collagenase solution supplemented with trypsin for the last 10 minutes of a 40 minute

digest. CFs were then rinsed with PBS, transferred to gelatin coated plates, and cultured in DMEM supplemented with 10% FBS, 1% penicillin/strep, and interferon gamma at 33°C in order to maintain the immortalized phenotype. Prior to experimental use, cells were replated in DMEM supplemented with 10% FBS and 1% penicillin/strep and grown at 37°C for 48 hours to deactivate the immortalized gene.

MΦ exfiltration was stimulated by intraperitoneal (IP) injection of 1mL of 4% thioglycollate media into C57BL/6 mice. After 72 hours, mice were sacrificed and the intraperitoneal cavity was flushed with 10 mLs of cold RPMI media to collect the cells. After washing in cold PBS, cells were plated in RPMI media supplemented with 10% FBS on tissue culture plastic and allowed to adhere for 1 hour. Following previous reports, non-adherent cells were then rinsed away and all remaining cells were taken to be macrophages (Zhang, Goncalves, and Mosser 2008).

Gel contraction assay

Isolated CFs (WT and *Cdh11*$^{-/-}$) were diluted in a 1.28 mg/mL collagen solution derived from PureCol (Advanced Biomatrix) to a final concentration of 250,000 cells/mL and were poured into a Teflon ring in a suspension well. After polymerizing for 1 hour, DMEM supplemented with 10% FBS and 1% penicillin/strep was added to flood the well and release the collagen gel from both the bottom of the well and the Teflon ring. Gels were imaged immediately after release and at multiple times over the next 48 hours. At each time point, gel areas were measured in ImageJ and normalized to the original gel area. For comparison of the impact of IgG2a and SYN0012 treatment, antibody was added to the cell/gel mixture at a final concentration of 20 μg/ml prior to pouring; media added to the well also contained 10 μg/ml of antibody (**Figure S11**).

qPCR

For assessment of *in vivo* transcription of specific pro-fibrotic and inflammatory genes of interest, hearts were isolated under RNAse-free conditions and immediately flash frozen. For isolation of mRNA, samples were subsequently thawed and lysed in TRIZOL with chloroform induced phase separation according to manufacturer's instructions. cDNA was synthesized using the Superscript IV kit (Invitrogen) using 500 ng of mRNA. Real time qPCR was used to amplify targets from the cDNA using a SYBR green master mix (BIO-RAD) and specific primer sets (**Table S1**). The BIO-RAD CFX96 C1000 system was used to quantify gene transcription in each sample, relative to *Gapdh*. For all of the *in vivo* transcription levels, post-MI samples were normalized to the average of all three and seven day Sham values (**Figure S14**).

Two-way ANOVAs were used to compare the relative transcription of targets of interests in IgG2a- and SYN0012-treated mice receiving MI and Sham animals that received neither MI nor antibody treatment at day three and day seven. An additional one-way ANOVA was run to compare the transcription levels of IgG2a and SYN0012 treated animals at 21 days after infarct and the average transcription of Sham animals. Two-way ANOVAs with Holm-Sidak's multiple comparison tests were also used to compare IgG2a and SYN0012 samples across all time points.

Table S1 qPCR primers

Target	Forward	Reverse
Gapdh	ATGACAATGAATACGGCTACAG	TCTCTTGCTCAGTGTCCTTG
Ctnt	AGGAGCTGATTTCCCTCAAAG	TTTCCTTCTCCCGCTCATTG
Cdh11, exon12	TCACTATCAAAGTCTGTGGCTG	CAAACAGCACAACGATGACC
Il6	CAAAGCCAGAGTCCTTCAGAG	GTCCTTAGCCACTCCTTCTG

F4/80	ACCACAATACCTACATGCACC	AAGCAGGCGAGGAAAAGATAG
Il1β	TCCTGTGTAATGAAAGACGGC	ACTCCACTTTGCTCTTGACTTC
Tnfα	AGACCCTCACACTCAGATCA	TGTCTTTGAGATCCATGCCG
Mmp3	CAGGAAGATAGCTGAGGACTTTC	GGTCAAATTCCAACTGCGAAG
Mmp13	GATTATCCCCGCCTCATAGAAG	TCTCACAATGCGATTACTCCAG
Tgfβ1	CCTGGGTTGGAAGTGGATC	TTGGTTGTAGAGGGCAAGG
αsma	GAGAAGCCCAGCCAGTCG	CTCTTGCTCTGGGCTTCA
Col1a1	CACCCTCAAGAGCCTGAGTC	GTTCGGGCTGATGTACCAGT
Fgf2	GGAGTTGTGTCTATCAAGGGAG	TGCCCAGTTCGTTTCAGTG
Vegfa1	AAAGCCAGCACATAGGAGAG	CGAGTCTGTGTTTTTGCAGG
Mrc1	ATGGATGTTGATGGCTACTGG	TTCTGACTCTGGACACTTGC
Cd14	CCTTTCTCGGAGCCTATCTG	CAACTTTCCTCGTCTAGCTCG
Arg1	AAGAATGGAAGAGTCAGTGTGG	GGGAGTGTTGATGTCAGTGTG

Quantification of IL-6 production by indirect ELISA

CFs were plated in each well of a 12 well plate (50,000 CFs/well) and allowed to adhere for 20 min prior to exposure to media containing between 0 and 50,000 MΦs. Cell suspensions were diluted to a final volume of 1.3 mL per well. We tested the interaction of cells (including MΦs alone) without antibody treatment, and then specifically compared CFs and a range of co-culture with IgG2a or SYN0012. For antibody treatments, samples were incubated with antibody (10 μg/ml) for 15 minutes before plating. After 48 hours in culture, conditioned media was removed from each well and IL-6 secretion was measured with a DuoSet mouse IL-6 ELISA (R&D Systems). After boiling, 100 μl of each sample was added in duplicate and compared against a provided standard (**Figure 7A-B**). Cells from these co-cultures were also lysed in TRIZOL for isolation of mRNA, cDNA synthesis, and analysis of transcription of specific gene targets by qPCR, as described above (**Figure 7C-E** and **Figure S15**).

One-way ANOVA with a post-hoc Holm-Sidak test to account for multiple comparisons was used to test for differences in expression of IL-6 and transcription of *MMP13* by untreated CFs with different CF:MΦ ratios. Two-way ANOVAs were run to compare the effect of increasing numbers of MΦs and treatment with either IgG2a or SYN0012 on IL-6 expression and gene transcription. The post-hoc Holm-Sidak method with an overall significance level of 0.05 was used to account for multiple comparisons within cell types and treatment groups.

References

Bersi, M R, R Khosravi, A J Wujciak, D G Harrison, and J D Humphrey. 2017. “Differential Cell-Matrix Mechanoadaptations and Inflammation Drive Regional Propensities to Aortic Fibrosis, Aneurysm or Dissection in Hypertension.” *Journal of the Royal Society, Interface* 14 (136): 1–31. https://doi.org/10.1098/rsif.2017.0327.

Chang, Sook Kyung, Ayano C. Kohlgruber, Fumitaka Mizoguchi, Xavier Michelet, Benjamin J. Wolf, Kevin Wei, Pui Y. Lee, et al. 2017. “Stromal Cell Cadherin-11 Regulates Adipose Tissue Inflammation and Diabetes.” *Journal of Clinical Investigation* 127 (9): 3300–3312. https://doi.org/10.1172/JCI86881.

Chen, Chen, Bai Lin Cong, Min Wang, Muhammad Abdullah, Xiao Long Wang, Yin Hua Zhang, Shun Ji Xu, and Lan Cui. 2018. “Neutrophil to Lymphocyte Ratio as a Predictor of Myocardial Damage and Cardiac Dysfunction in Acute Coronary Syndrome Patients.” *Integrative Medicine Research* 7 (2): 192–99. https://doi.org/10.1016/j.imr.2018.02.006.

Gao, Erhe, Yong Hong Lei, Xiying Shang, Z. Maggie Huang, Lin Zuo, Matthieu Boucher, Qian Fan, J. Kurt Chuprun, Xin L. Ma, and Walter J. Koch. 2010. “A Novel and Efficient Model of Coronary Artery Ligation and Myocardial Infarction in the Mouse.” *Circulation Research* 107 (12): 1445–53. https://doi.org/10.1161/CIRCRESAHA.110.223925.

Golden, H B, D Gollapudi, F Gerilechaogetu, J Li, R J Cristales, X Peng, and D E Dostal. 2012. “Isolation of Cardiac Myocytes and Fibroblasts from Neonatal Rat Pups.” *Methods Mol Biol* 843: 205–14. https://doi.org/10.1007/978-1-61779-523-7_20.

O’Connell, Timothy D., Manoj C. Rodrigo, and Paul C. Simpson. 2007. “Isolation and Culture of Adult Mouse Cardiac Myocytes.” In *Cardiovascular Proteomics*, 271–96. New Jersey: Humana Press. https://doi.org/10.1385/1-59745-214-9:271.

Rocha, Kelvin R., Anthony J. Yezzi, and Jerry L. Prince. 2007. “A Hybrid Eulerian-Lagrangian Approach for Thickness, Correspondence, and Gridding of Annular Tissues.” *IEEE Transactions on Image Processing* 16 (3): 636–48. https://doi.org/10.1109/TIP.2007.891072.

Rose, Shawn, Alexander Misharin, and Harris Perlman. 2012. “A Novel Ly6C/Ly6G-Based Strategy to Analyze the Mouse Splenic Myeloid Compartment.” *Cytometry Part A* 81A (4): 343–50. https://doi.org/10.1002/cyto.a.22012.

Yezzi, Anthony J, and Jerry L Prince. 2003. “An Eulerian PDE Approach for Computing Tissue Thickness.” *IEEE Transactions on Medical Imaging* 22 (10): 1332–39. https://doi.org/10.1109/TMI.2003.817775.

Zhang, X, R Goncalves, and D M Mosser. 2008. “The Isolation and Characterization of Murine Macrophages.” *Curr Protoc Immunol* Chapter 14: Unit 14 1. https://doi.org/10.1002/0471142735.im1401s83.

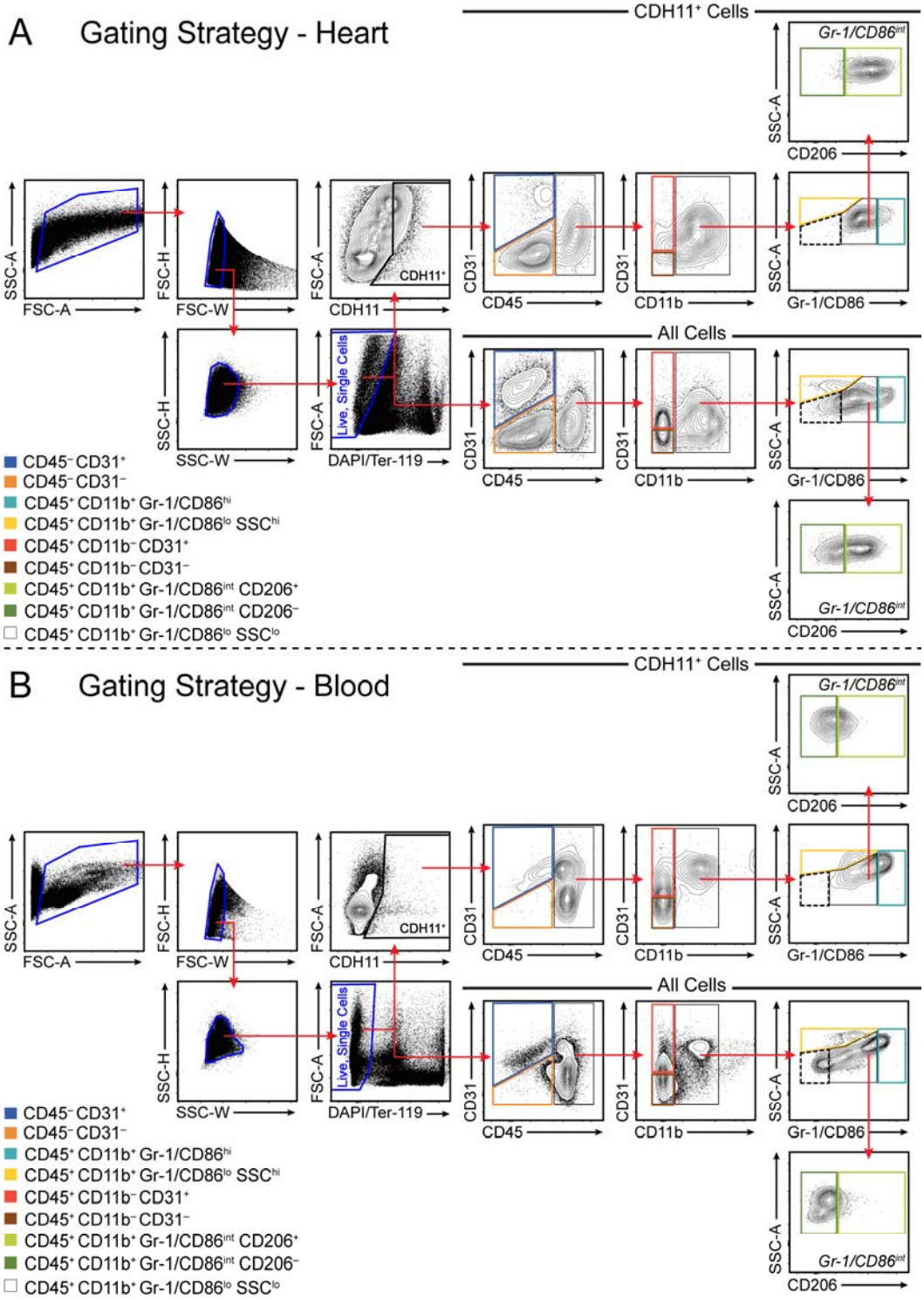

Figure S1. Flow cytometry gating strategy. Live single cells were identified from all measured events in the heart (**A**) and blood (**B**). Cells were gated into cardiac endothelial cells (blue), cardiac mesenchymal cells (orange), and bone-marrow derived cells (BMDCs). BMDCs were further gated into bone marrow-derived proangiogenic cells (red), non-myeloid lineage BMDCs (brown; lymphocytes), and myeloid lineage cells including neutrophils (light blue), eosinophils (yellow), monocytes (white/dashed) and macrophages. Macrophage polarization was assessed by defining M1-like macrophages (dark green) and M2-like macrophages (light green). Gating was applied to all events (bottom rows) and CDH11⁺ cells (top rows) and is shown for representative samples at seven days after infarct.

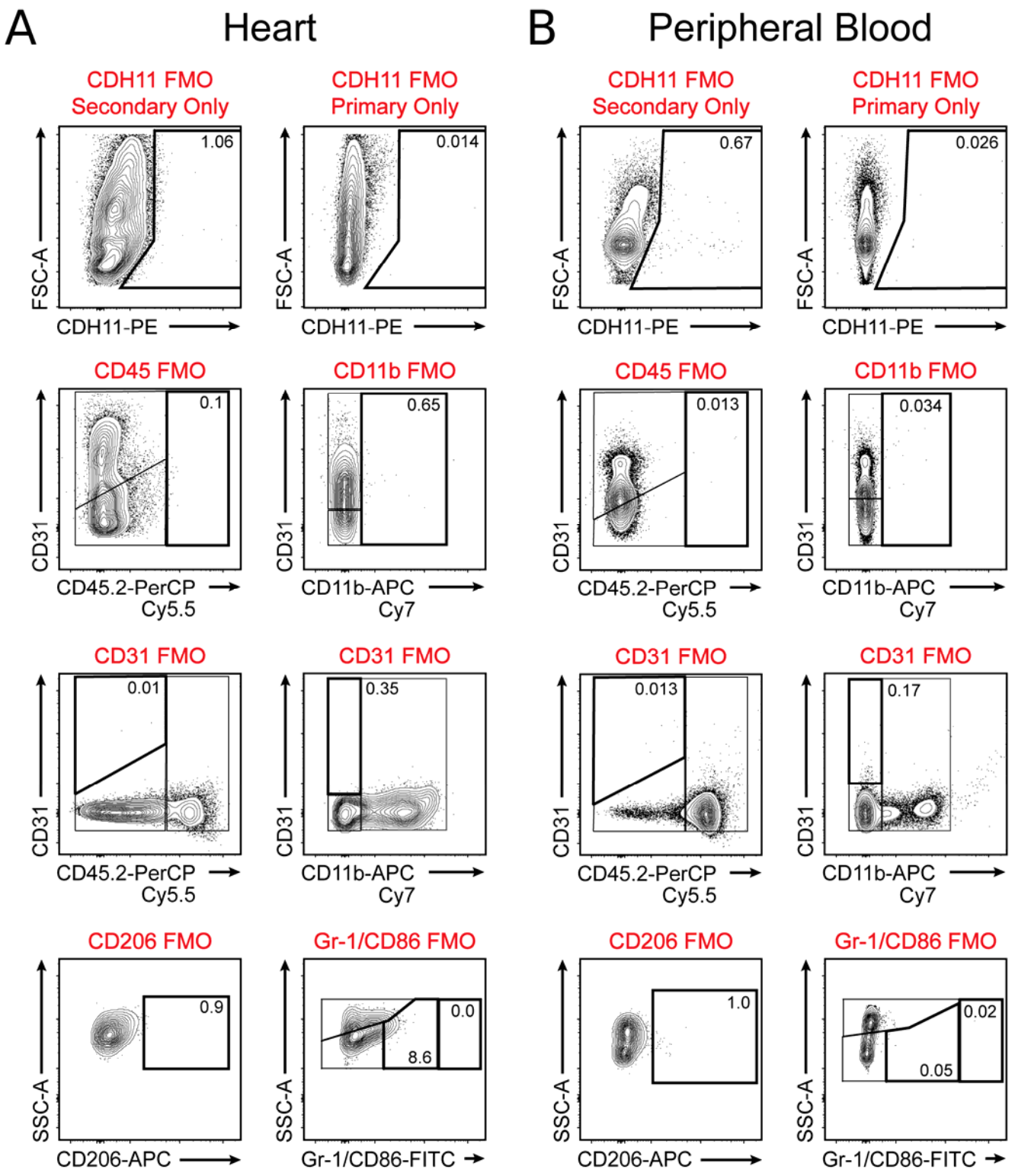

Figure S2. Fluorescence minus one (FMO) controls for flow cytometry analysis. FMO controls for each antibody used in the flow cytometric analyses indicates the placement of gates defining each of the primary cell populations in the heart (**A**) and peripheral blood (**B**). Inset numbers show the percent of parent population events that fall within each gate.

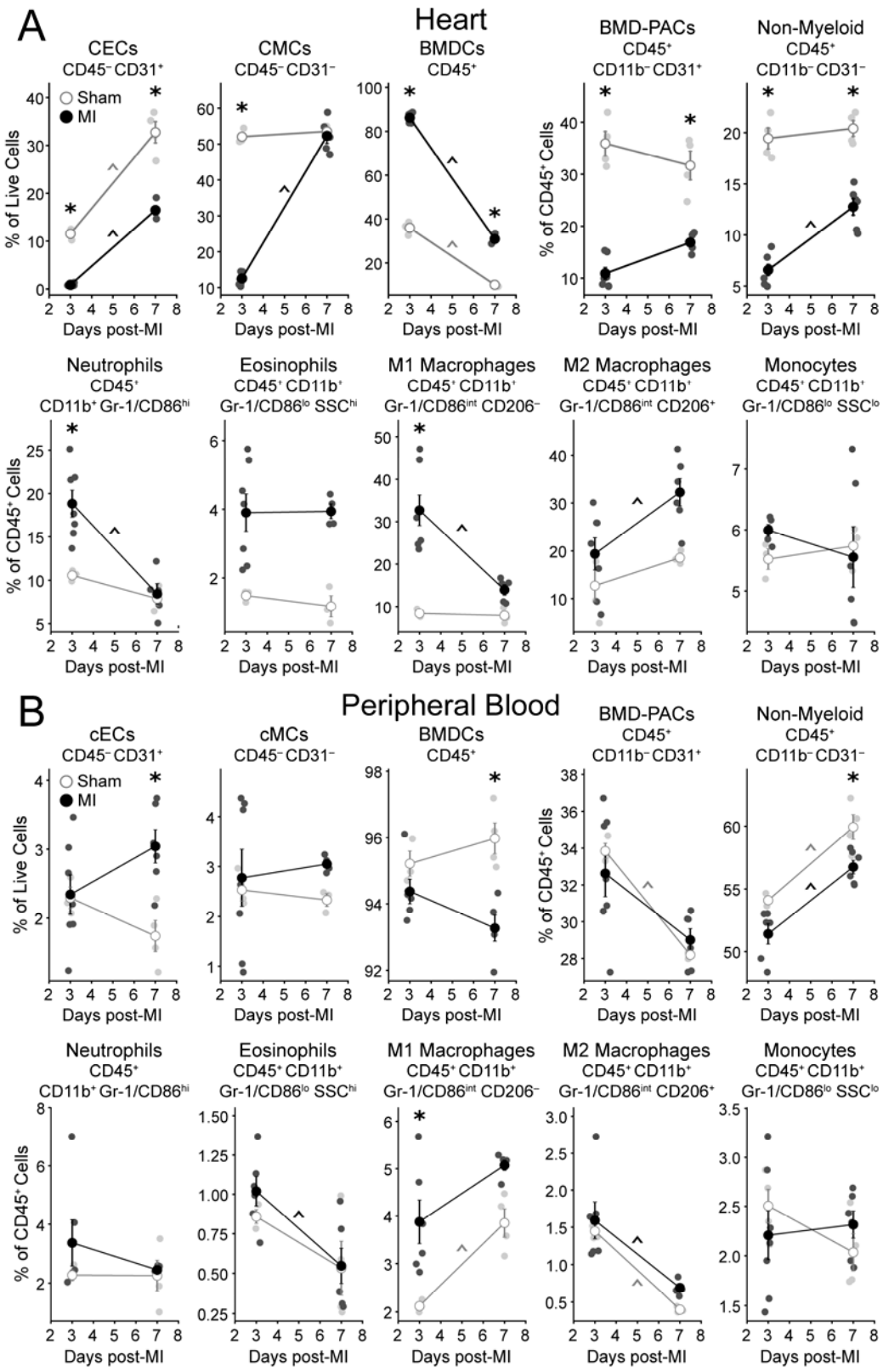

Figure S3. Changes in resident and bone marrow derived cell expression after MI. Flow cytometric analysis allows for quantification of each of the identified non-cardiomyocyte cell populations as a percentage of all live single cell events in the heart (**A**) and peripheral blood (**B**) after MI. * $p < 0.05$ between Sham and MI at the same time, ^ $p < 0.05$ over time; n = 3-7 per group.

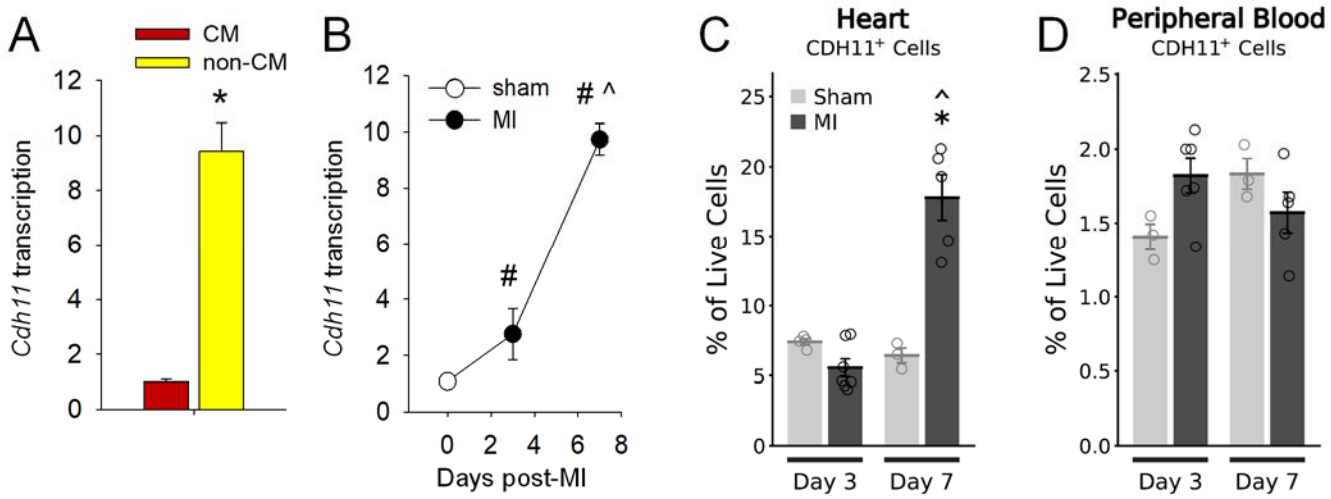

Figure S4. CDH11 expression is increased in the heart post-MI. Transcription of *Cdh11* occurs primarily in non-CM cells (**A**) and increases up to maximal expression (~10-fold higher than Sham) at day seven after MI (**B**). Flow cytometric analysis allows for quantification of CDH11$^+$ cells as a percentage of all live single cell events, in the heart (**C**) and peripheral blood (**D**) after MI. For **A-B**: * $p < 0.05$ between cell types, # $p < 0.05$ relative to Sham, ^ $p < 0.05$ relative to previous time point; For **C-D**: * $p < 0.05$ between Sham and MI at the same time, ^ $p < 0.05$ over time; n = 3-7 per group.

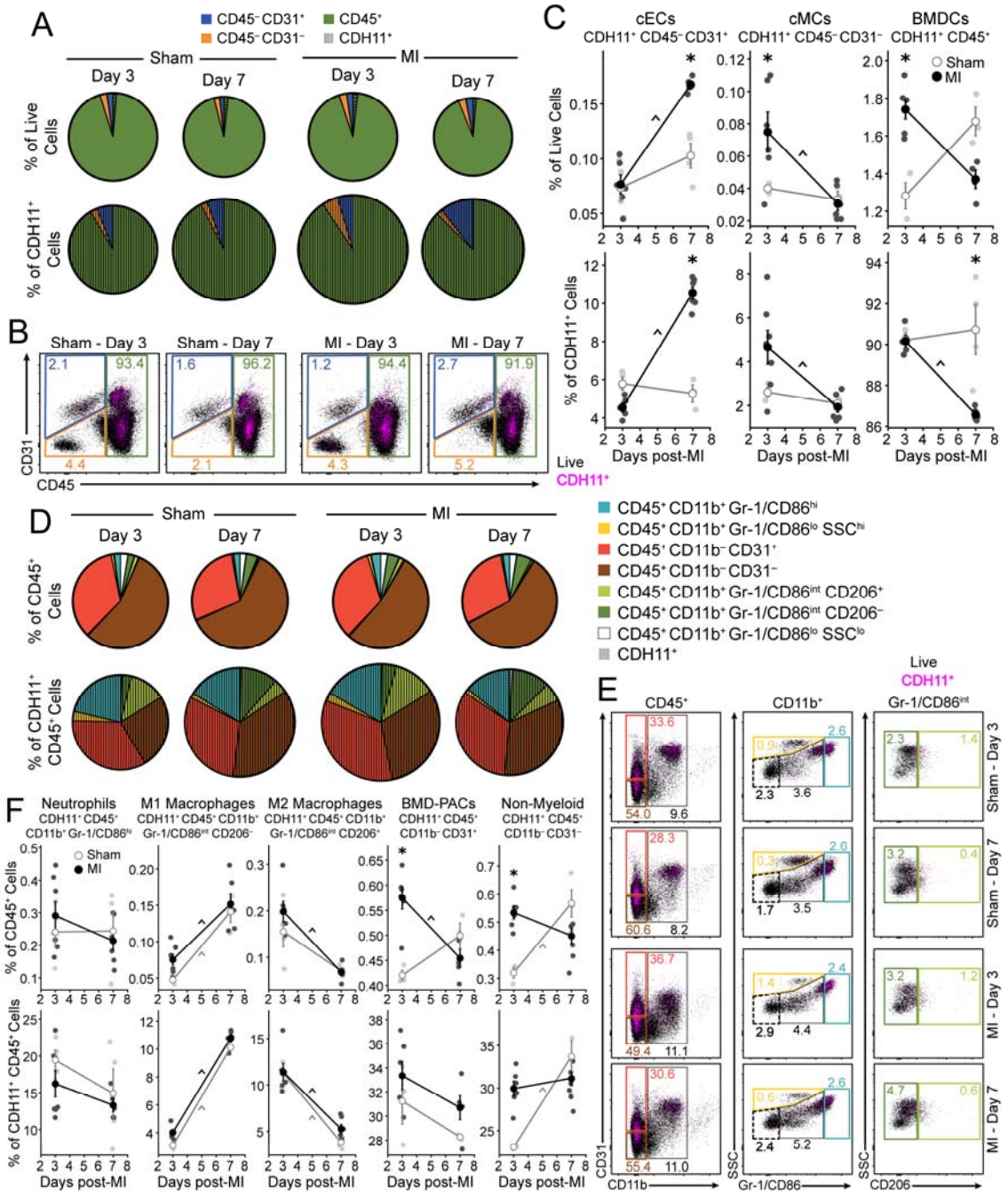

Figure S5. CDH11 expression in the blood is largely unaffected post-MI. Flow cytometric analysis reveals that circulating endothelial (cEC), mesenchymal (cMC), and bone marrow derived (BMDC) cell populations have minimal baseline CDH11 expression and are largely unaffected post-MI (hatched wedges). Pie chart radii (**A**) are scaled by either the number of live single cells (top row) or the number of CDH11$^+$ cells (bottom row) relative to that in Sham hearts at day three. Representative dot plots (**B**) show CDH11 expression (magenta) within each cell population (colored gates). CDH11$^+$ cells (**C**) within each population are shown as either a percentage of live cells (top row) or of all CDH11$^+$ cells. While CDH11 expression was low (<2% of total cells), the percent of CDH11$^+$ cells that are cECs is increased and that are BMDCs is decreased, relative to Sham, at day seven post-MI. BMDC subpopulations (**D**) revealed little CDH11 expression with little difference between Sham and MI. Representative dot plots (**E**) show CDH11 expression (magenta) within each subpopulation (colored gates). Though CDH11 expression was low in each BMDC subpopulation (<1% of CD45$^+$ cells), there was an increase in CDH11$^+$ BMD-PACs and CDH11$^+$ non-myeloid BMDCs at three days post-MI, with non-myeloid BMDCs comprising significantly more of all CDH11$^+$ BMDCs than Sham at day three. Percentages of each population, relative to all live cell events, are denoted within colored gates. * $p < 0.05$ between Sham and MI at the same time, ^ $p < 0.05$ over time; n = 3-7 per group.

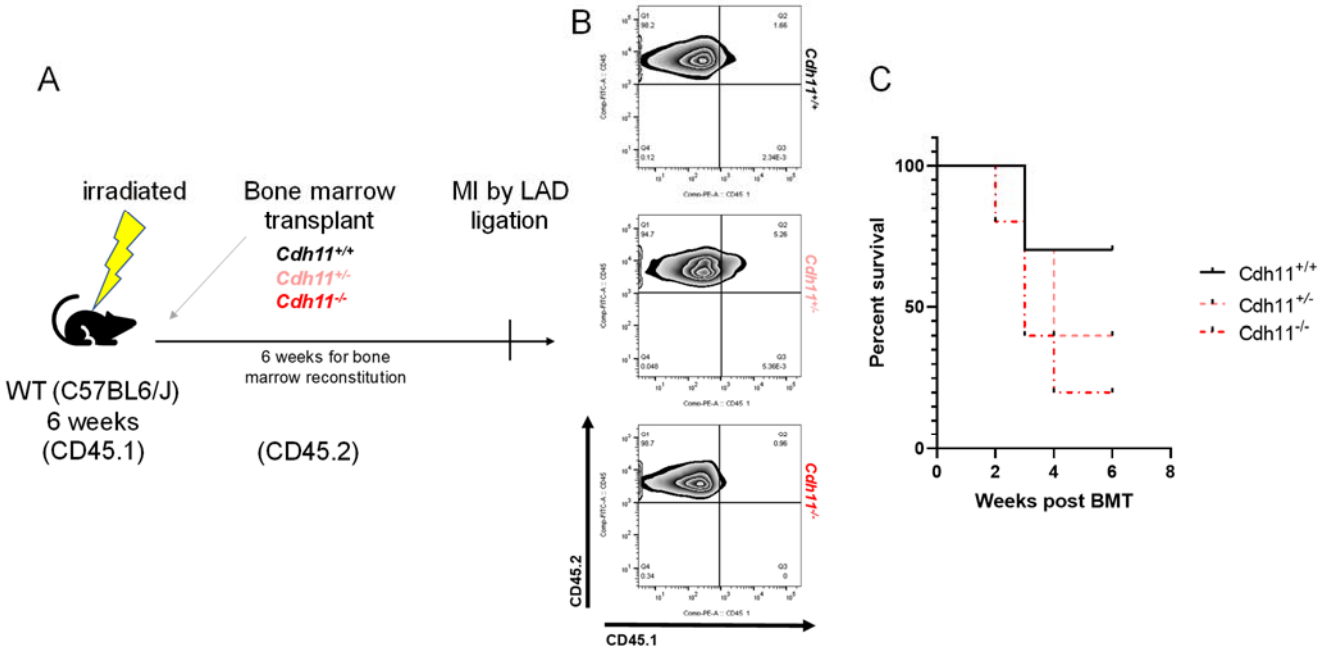

Figure S6: Experimental protocol for bone marrow transplantation. Schematic of experimental protocol for bone marrow transplantation from *Cdh11* transgenic donors (CD45.2) into lethally irradiated C57BL6/J recipients (CD45.1; B6.SJL-*Ptprc*^{a}*Pepc*^{b}/BoyJ) (**A**). Flow cytometry of CD45.1 and CD45.2 expression in the bone marrow after 6 weeks of reconstitution was used to confirm successful bone marrow transplantation (**B**). Despite successful transplantation, fewer mice with *Cdh11* transgenic bone marrow (e.g., *Cdh11*$^{+/-}$ and *Cdh11*$^{-/-}$) survived to the point of complete bone marrow reconstitution and the subsequent MI surgery (**C**).

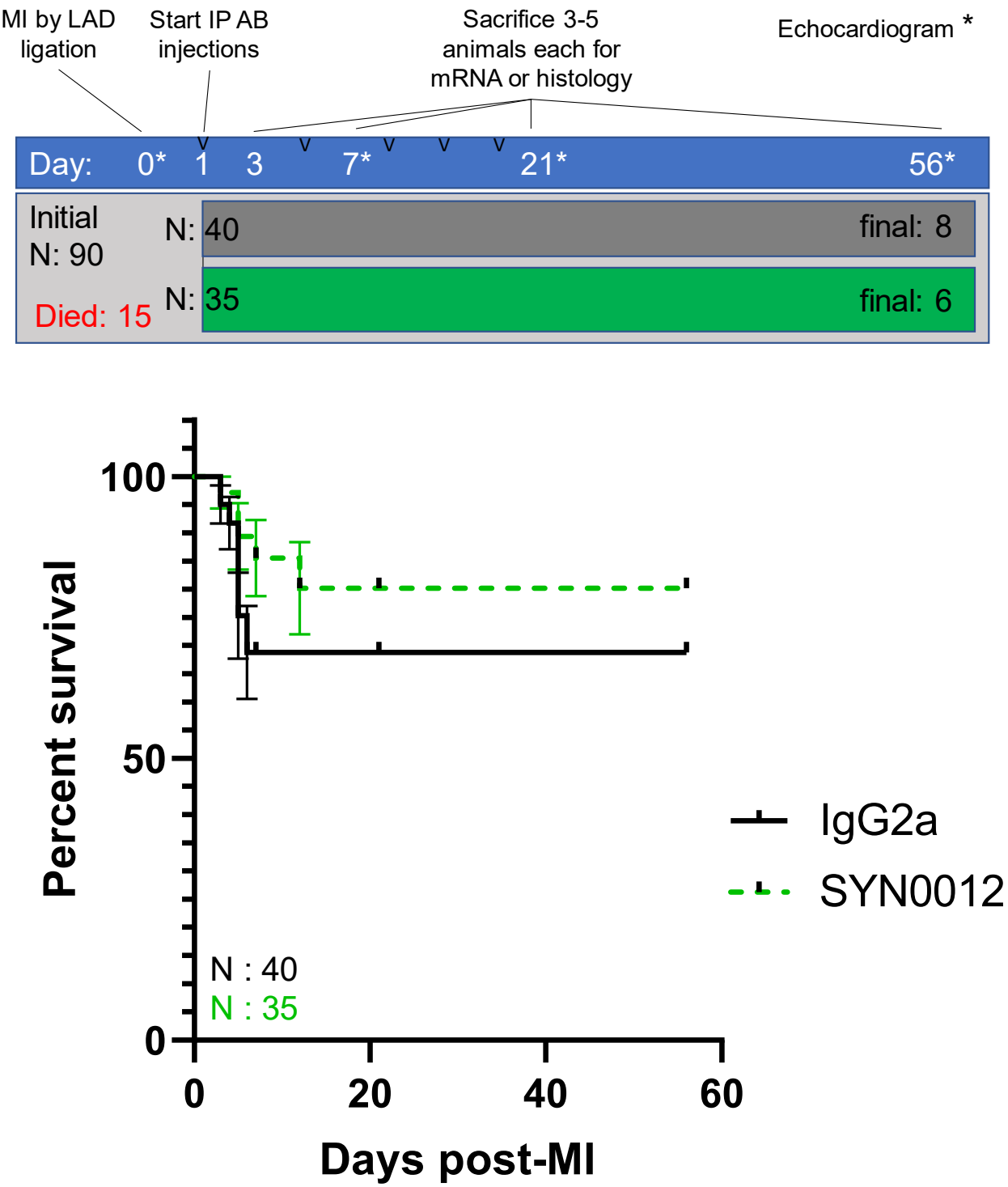

Figure S7: CDH11 blockade improves survival after MI. Experimental time course of antibody treatment, with injection days marked with 'v', and days of echocardiogram marked with '*'. Following MI, fewer animals receiving SYN0012 treatment died than those receiving IgG2a. Error bars represent standard error (SE).Though survival was improved, the findings were not statistically significant with a value of $p = 0.20$ following a Gehan-Breslow-Wilcoxon test.

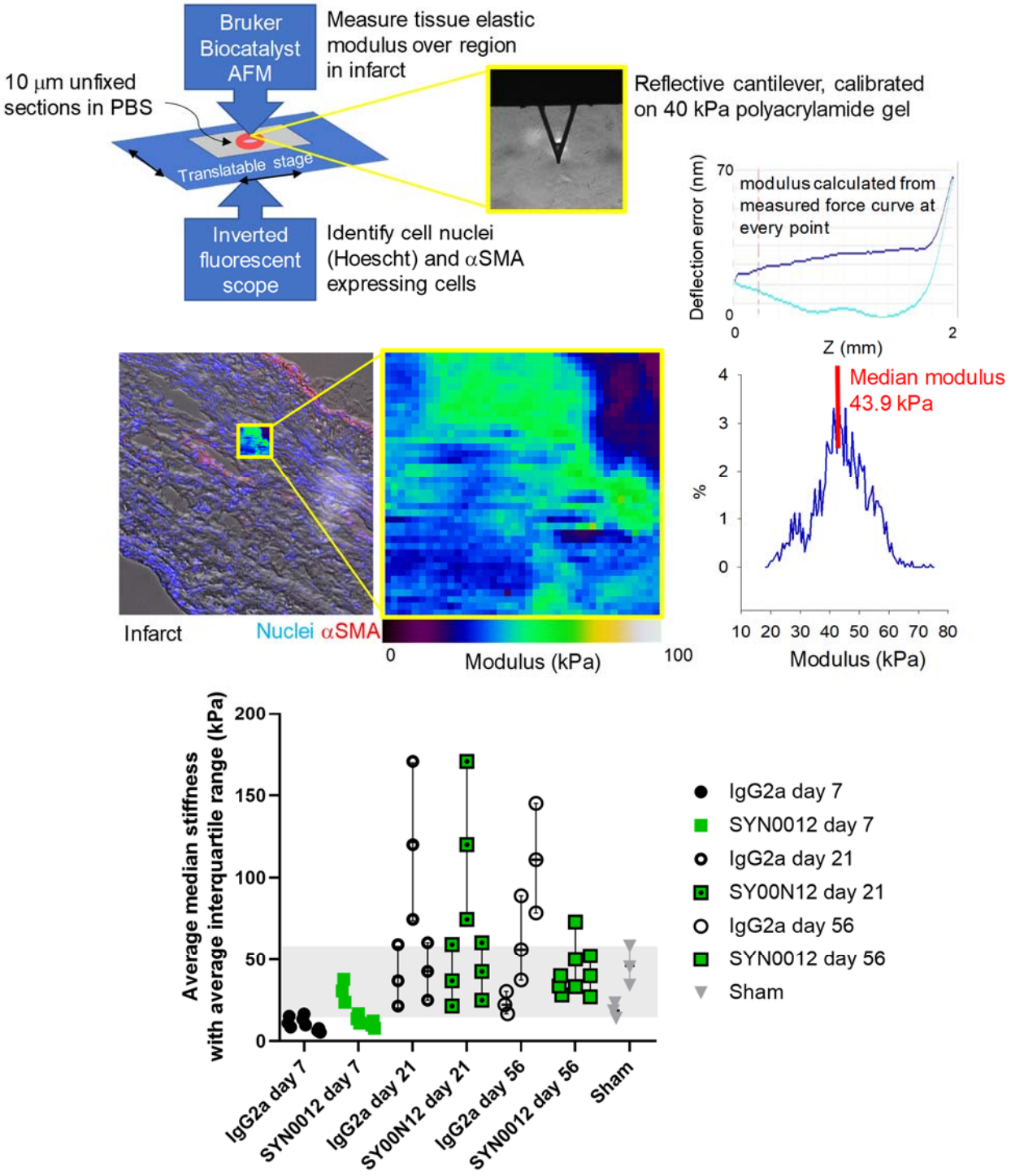

Figure S8: Atomic force microscopy and stiffness measurement pipeline. Schematic of atomic force microscopy (AFM) and fluorescent microscope arrangement, with a callout image of the pyramidal probe cantilever (top panel; yellow). A typical indentation curve from PeakForce QNM mode is also shown (top right). Representative area scan from 10x10μm^2 of infarcted tissue is shown with fluorescently labeled nuclei (blue) and αSMA$^+$ cells (red). Inset shows representative stiffness (modulus) colormap (middle let panel) and a corresponding histogram shows the distribution and median of measured moduli (middle right panel). For each mouse, tissue sections were analyzed by AFM and the average median stiffness and interquartile range was averaged from 6-8 scans per mouse.

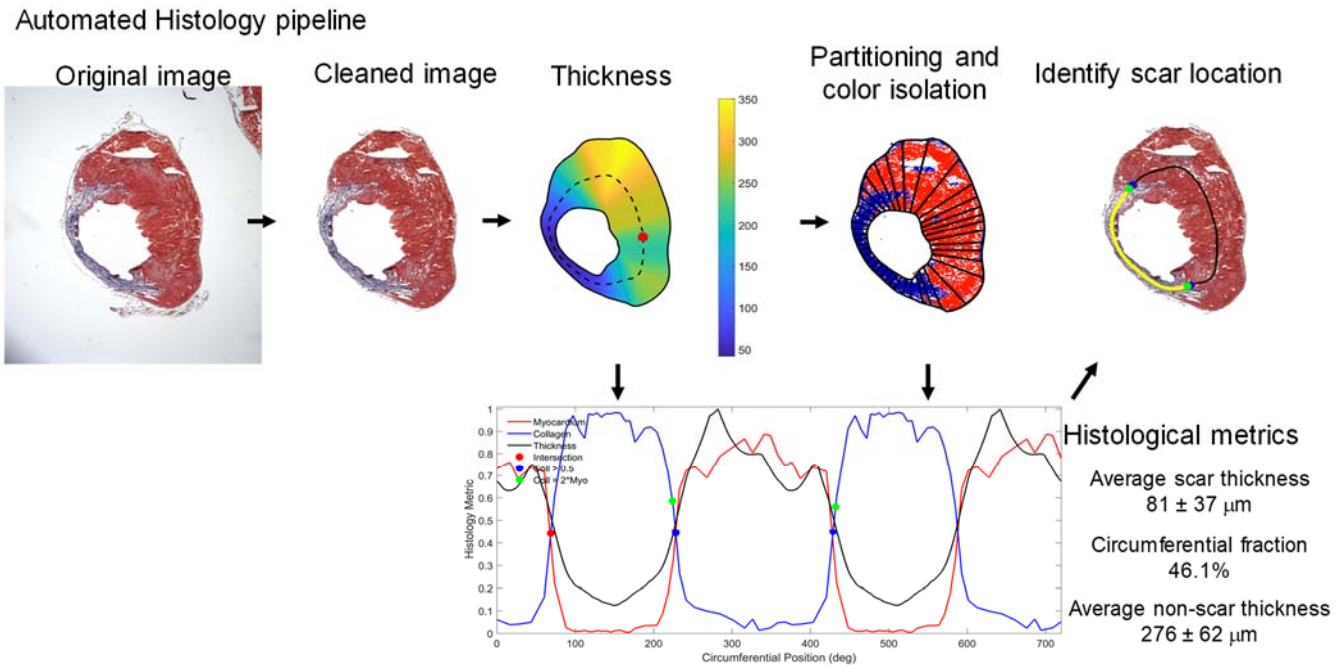

Figure S9: Semi-automatic histological image analysis pipeline. Masson's trichrome stained short-axis sections of infarcted hearts were analyzed in order to quantify infarct morphology such as infarct length as a circumferential percentage and average infarct thickness. Following background removal, thickness between the identified inner and outer boundaries is computed. A total of 40 circumferential partitions are defined, and colorimetric segmentation of red and blue pixels is performed (shown as pseudo-colored image). Infarct borders are then defined based on intersections between red/blue area fractions (bottom panel); infarct and non-infarct morphology (length, thickness, variance, etc.) is computed following semi-automatic identification of infarct borders.

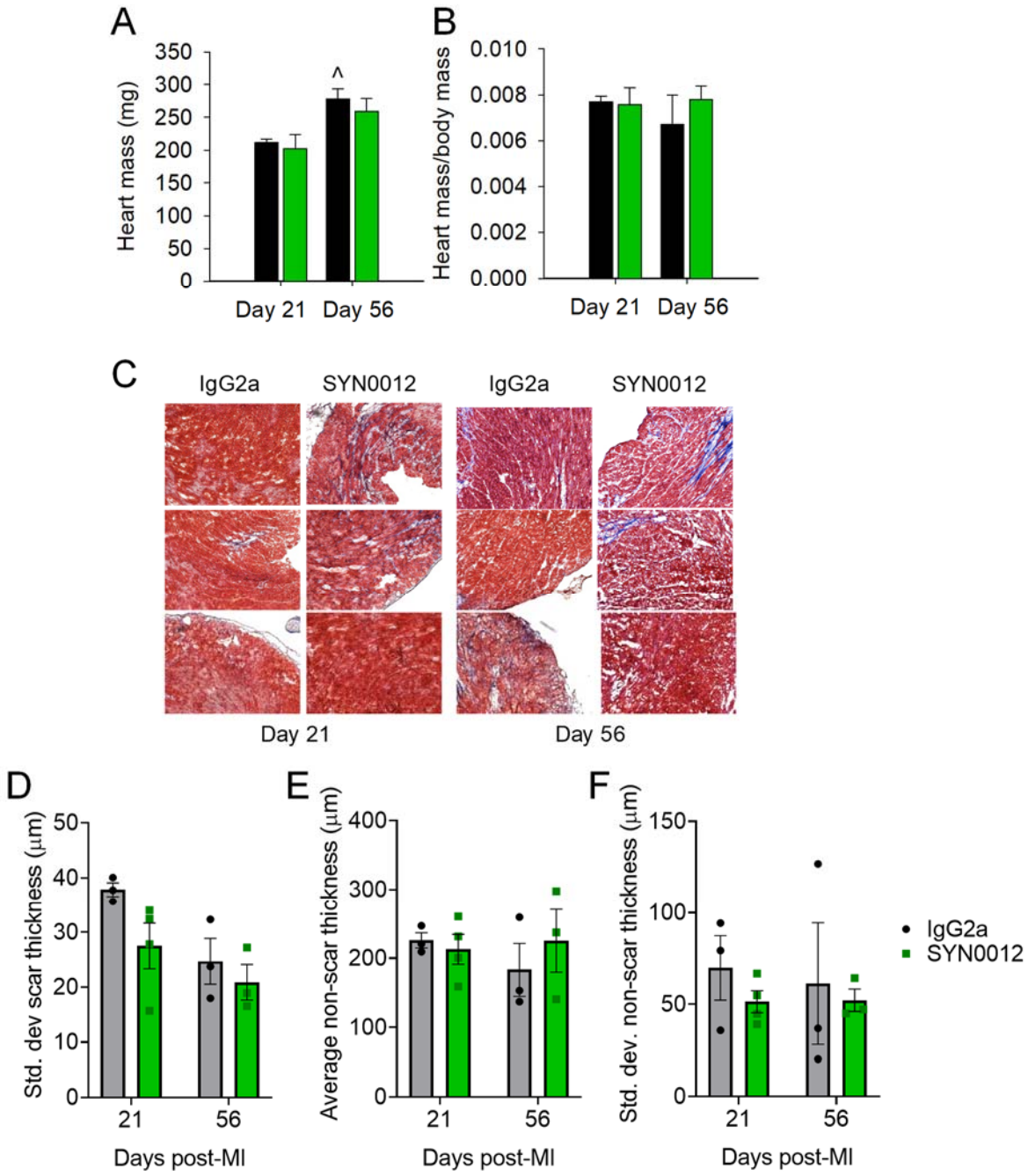

Figure S10. CDH11 blockade has little effect on cardiac hypertrophy and interstitial fibrosis. Quantification of heart mass (**A**) and heart to body mass ratio (**B**) revealed minimal differences aside from a significant increase in heart mass from 21 to 56 days in IgG2a-treated hearts that was not observed with SYN0012 treatment. Visual inspection of Masson's Trichrome staining of distant regions of the myocardium (three hearts per group shown) revealed no difference in remote interstitial fibrosis in each of the three (**C**) and there was also no significant difference in the measured standard deviation of the scar thickness and average and standard deviation of the non-scar thickness (**D-F**) at days 21 and 56 between treatments. ^ $p < 0.05$ between timepoints; $n \geq 3$ per group.

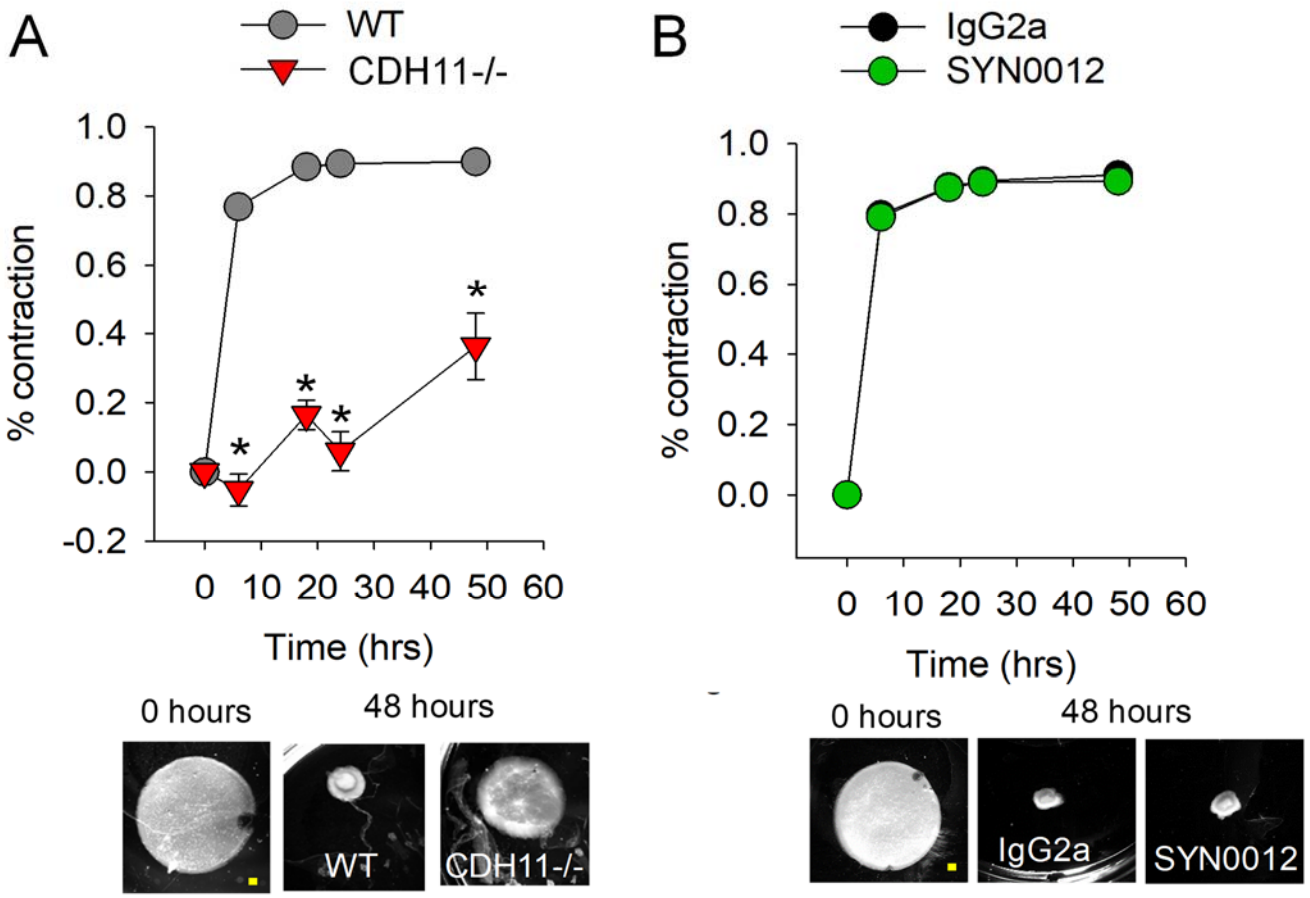

Figure S11: CDH11 modulates cardiac fibroblast contraction. Cardiac fibroblasts (CFs) isolated from *Cdh11*$^{-/-}$ mice exhibit a reduction in contractile ability relative to *Cdh11*$^{+/+}$ control CFs, as shown by a reduction in collagen gel contraction (**A**). Pharmacologic targeting of CDH11 in WT (C57BL6/J) CFs with SYN0012 treatment does not affect CF contractility and gel contraction (**B**). Yellow scale bar represents 1 mm. * $p < 0.05$ between groups at the same time; n = 3 per group.

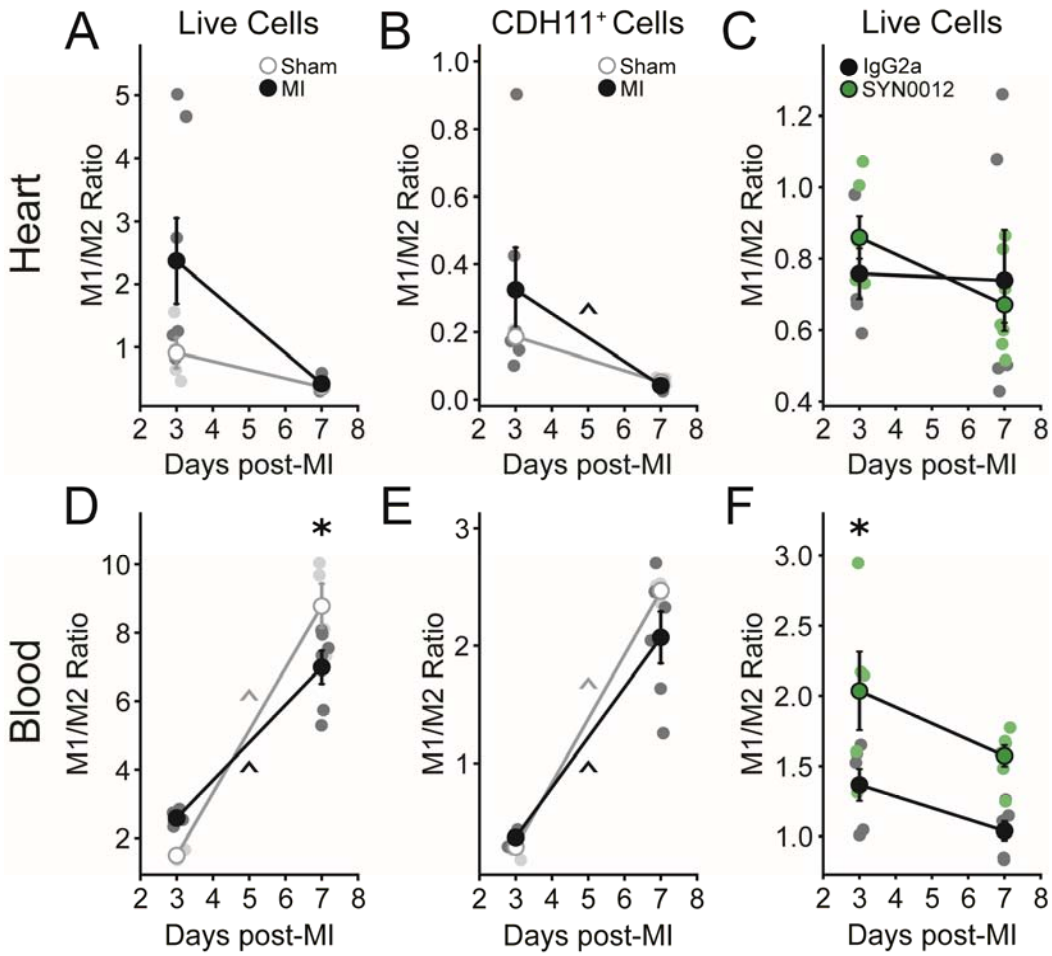

Figure S12. Ratios of macrophage polarization are affected by MI. Flow cytometric analysis reveals that the ratio of M1:M2-like macrophages in the heart was increased, though not significantly different, relative to Sham at day three when calculated as a percentage of all live cells (**A**) and all CDH11$^+$ cells (**B**). Cardiac M1:M2-like ratios were not different between IgG2a and SYN0012 treatments (**C**). M1:M2-like ratios based on all live cells in the peripheral blood significantly increased in Sham animals between day three and seven, and was larger than MI samples at day seven (**D**), but was not significantly affected in the CDH11$^+$ populations (**E**). SYN0012 treatment resulted in a higher M1:M2-like macrophage ratio that IgG2a after three days (**F**) which may suggest that CDH11 blockade alters macrophage recruitment to the heart after MI. * $p < 0.05$ between either Sham and MI or antibody treatments at the same time, ^ $p < 0.05$ over time; n = 3-7 per group.

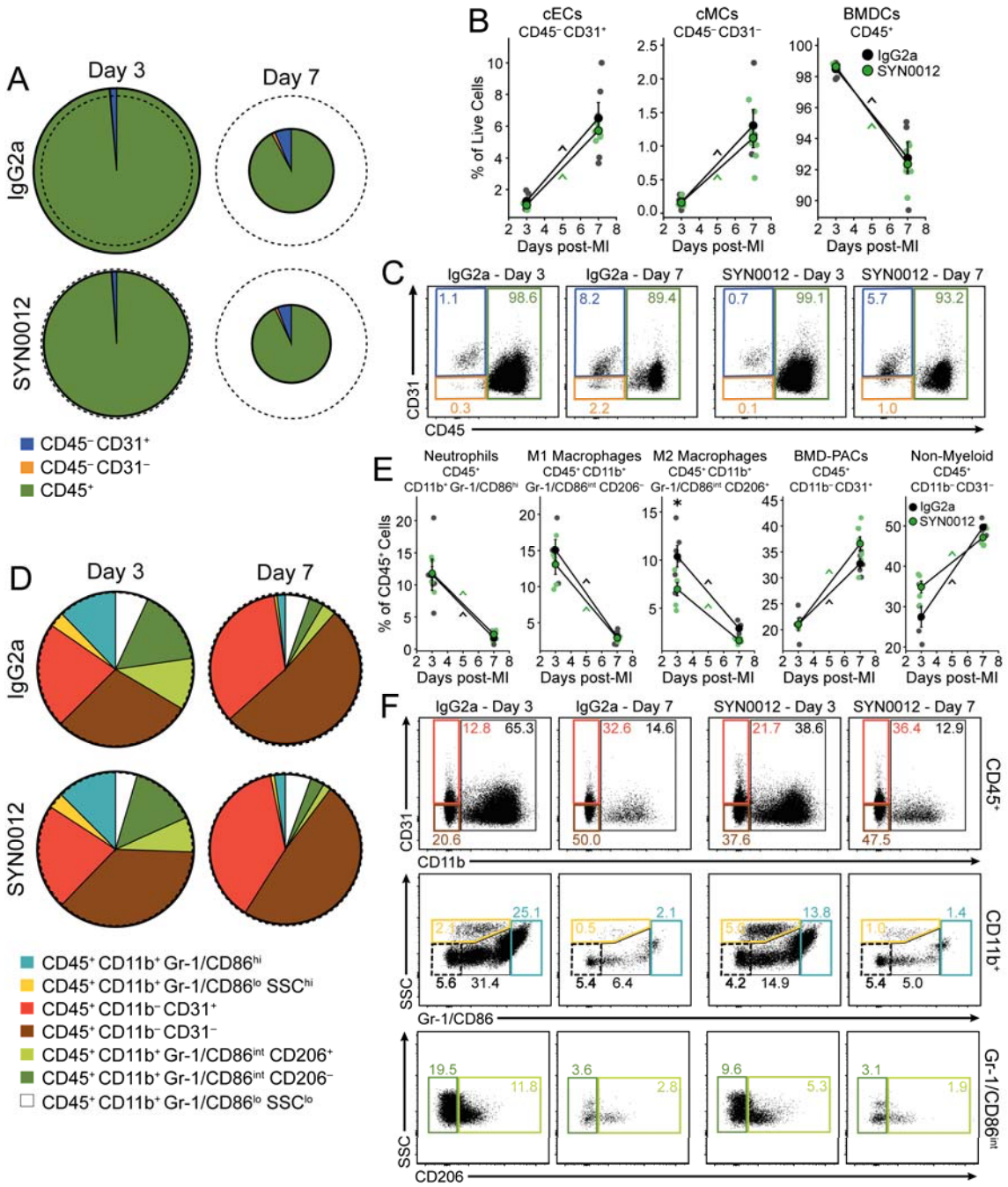

Figure S13. CDH11 blockade has little effect on circulating cell populations post-MI. Flow cytometric analysis reveals that CDH11 blockade by SYN0012 does not alter the percentages of circulating endothelial (cEC), mesenchymal (cMC), and bone marrow derived (BMDC) cells in the blood post-MI, relative to IgG2a, but differences are seen over time (**A-B**). Pie chart radii are scaled by the number of live single cells for each treatment and time, relative to Sham blood samples at day three (denoted by dotted circles). Representative dot plots (**C**) show changes in expression of each cell population (colored gates). Separation of BMDC subpopulations (**D**) revealed that SYN0012 significantly decreases circulating M2-like macrophages and shows a trend toward increasing non-myeloid BMDCs (lymphocytes) at day three (**E**). Differences were observed over time in all populations. Representative dot plots (**F**) show changes in expression of each BMDC subpopulation (colored gates). Percentages of each population, relative to all live cell events, are denoted within colored gates. * $p < 0.05$ between treatments at the same time, ^ $p < 0.05$ over time; n = 3-7 per group.

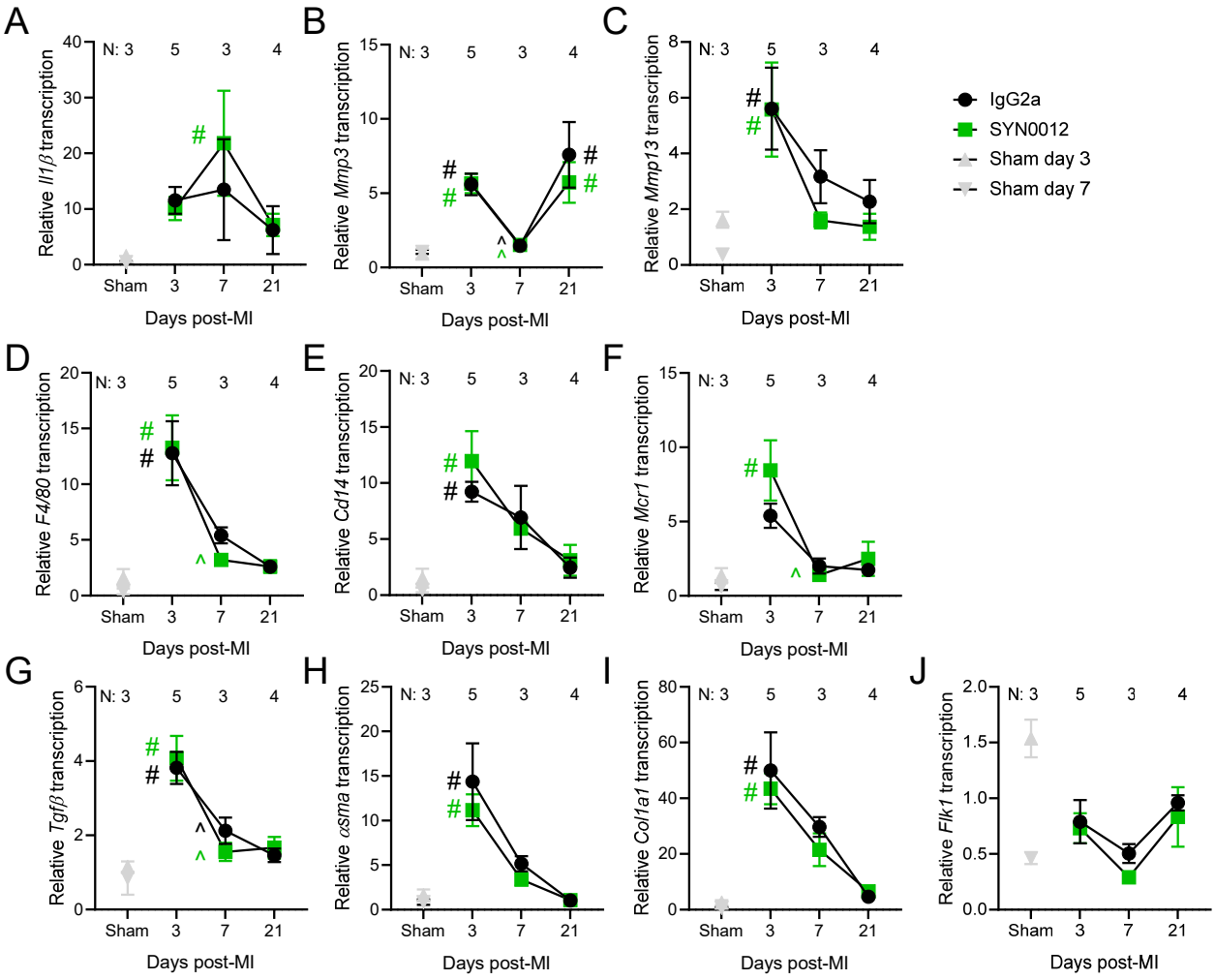

Figure S14: MI induces transcriptional changes in pro-inflammatory and pro-fibrotic genes. qPCR was used to characterize the time-dependent transcriptional changes in multiple proinflammatory and profibrotic genes of interest. In particular, transcriptional profiles for *Il1β* (**A**), *Mmp3* (**B**), *Mmp13* (**C**), *F4/80* (**D**), *Cd14* (**E**), *Mrc1* (**F**), *Tgfβ* (**G**), *αsma* (**H**), *Col1a1* (**I**), and *Flk1* (**J**) are shown. * $p < 0.05$ between treatments, # $p < 0.05$ relative to Sham, ^ $p < 0.05$ relative to previous time point.

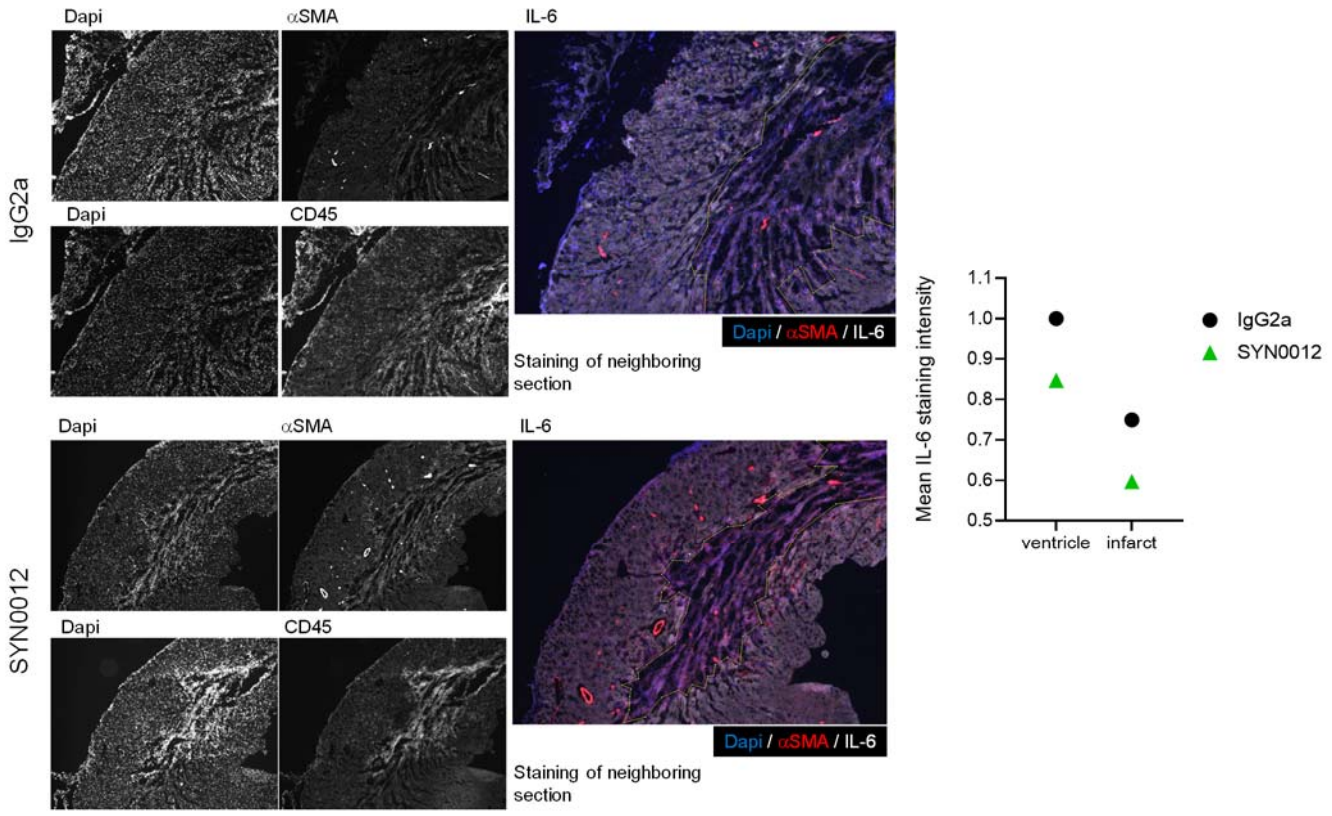

Figure S15: Immunostaining of infarct and peri-infarct regions of IgG2a and SYN0012 treated heart. Neighboring sections were stained with IL-6, aSMA and CD45 antibodies, along with Dapi, to colocalize expression of IL-6 with myofibroblasts and bone-marrow derived cells. The area without CMs was deemed the infarct area (outlined in yellow in the far right panels) and the average IL-6 signal intensity in this region was quantified and compared to the average intensity from the whole area of the ventricular myocardium from these images.

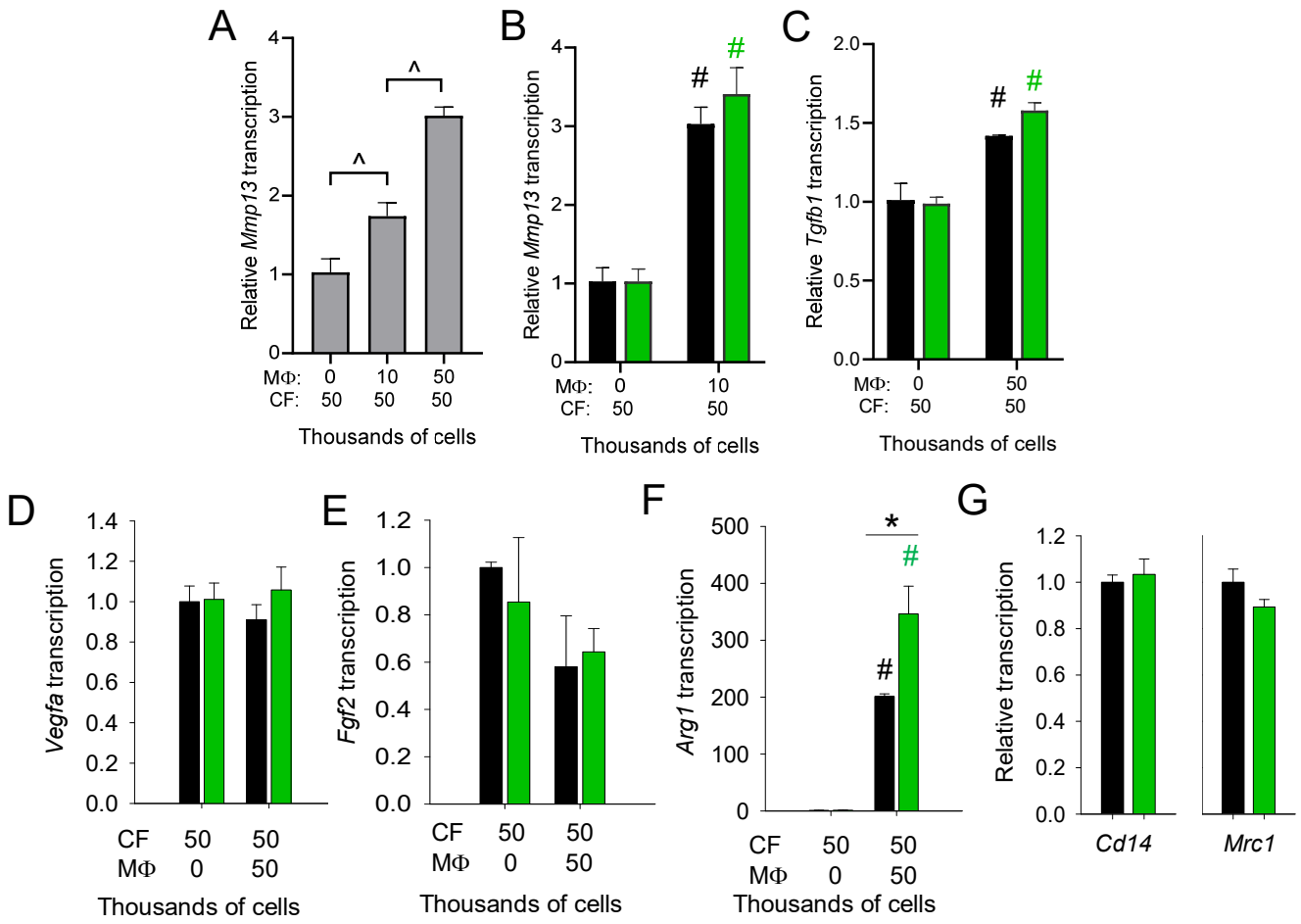

Figure S16: Effect of CF-MΦ co-culture on transcription of profibrotic, proangiogenic, and macrophage polarization markers. *MMP13* transcription was significantly increased with macrophage number (**A**). *MMP13* (**B**) and *Tgfb1* (**C**) transcription both increased with MΦ coculture, but were not significantly altered by SYN0012 treatment. There were no transcriptional differences in proangiogenic growth factors *Vegfa1* (**D**) and *Fgf2* (**E**) with SYN0012 treatment. Additionally, *Vegfa1* transcription was not dependent upon MΦ concentration, whereas *Fgf2* showed a trend toward decreasing transcription with increasing number of MΦs in the co-culture. Conversely, there was a significant increase in *Arg1* transcription – a marker of M2 macrophage polarization – with SYN0012 treatment (**F**), but no difference in M1 and M2 macrophage markers *Cd14* and *Mrc1*, respectively (**G**). * $p > 0.05$ between treatments, # $p > 0.05$ relative to CF-only group; n = 3-4 for all samples.

Supplemental Material

CADHERIN-11 BLOCKADE REDUCES INFLAMMATION-DRIVEN FIBROTIC REMODELING AND IMPROVES OUTCOMES AFTER MYOCARDIAL INFARCTION

Schroer, Cadherin-11 regulates fibrotic remodeling after MI

Alison K. Schroer, PhD[a], Matthew R. Bersi, PhD[a], Cynthia R. Clark, PhD[a], Qinkun Zhang, MD[b], Lehanna H. Sanders, PhD[b], Antonis K. Hatzopoulos, PhD[b], Thomas L. Force, MD[b], Susan M. Majka, PhD[c], Hind Lal, PhD[b], and W. David Merryman, PhD[a]

[a] Department of Biomedical Engineering, [b] Department of Cardiovascular Medicine, [c] Department of Allergy, Pulmonary, and Critical Care Medicine, Vanderbilt University, Nashville, TN, USA 37253

For Correspondence:
W. David Merryman
Room 9445D MRB4
2213 Garland Ave
Nashville, TN 37212
P: 615.322.7219
F: 615.322.6541
E: david.merryman@vanderbilt.edu

Detailed Methods

Mice

All animal procedures were approved by the Institutional Animal Care and Use Committee at Vanderbilt University. Myocardial infarction (MI) was induced by permanent ligation of the left anterior descending (LAD) coronary artery, as previously described (Gao et al. 2010). Briefly, mice were anesthetized by 2% isoflurane inhalation, without ventilation, and a small skin incision was made over the left chest. After dissection and retraction of the pectoral major and minor muscles, the 4th intercostal space was exposed and a small hole was made to open the pleural membrane and pericardium. The heart was then gently popped out through the hole and the LAD was ligated ~3 mm from its origin using a 6-0 silk suture. Successful ligation was confirmed by pale coloration of the anterior wall of the left ventricle. Following LAD ligation, the heart was placed back into the intra-thoracic space, air was evacuated from the thoracic cavity, and the muscle and skin was sutured closed. MI was performed in 12 to 16 week old male *Cadherin-11* deficient mice (*Cdh11*$^{+/+}$, *Cdh11*$^{+/-}$, *Cdh11*$^{-/-}$) or WT male mice (C57BL/6J; Jackson Laboratories). All mice were given pre- and post-operative analgesic of 5 mg/kg ketoprofen every 24 hours for 72 hours.

For antibody treatments, mice were administered either 10 mg/kg of a cadherin-11 (CDH11) functional blocking antibody (SYN0012; with permission from Roche) or an isotype control antibody (IgG2a) resuspended in sterile saline. Antibodies were delivered by intraperitoneal (IP) injection every four days, beginning one day after surgery, with the last treatment given on day 17 after infarct. Comparisons between survival curves were evaluated using the Gehan-Breslow-Wilcoxon test.

Isolation of cardiomyocyte and non-cardiomyocyte cells

Live cardiac cells were isolated from mouse hearts as previously described (O'Connell, Rodrigo, and Simpson 2007). Briefly, slow perfusion of the heart with a collagenase solution was used to digest the ECM and isolate intact cardiomyocytes (CMs) and non-CMs from hearts. Cells were separated into CM and non-CM fractions by centrifugation for 10 min at 90 g and lysed in TRIZOL for analysis of *Cdh11* transcription. Transcription of *Cdh11* in both cell types was normalized to CM expression and compared with a Student's t-test.

Identification of non-CM cell types by flow cytometry

Composition of cell types in the heart and the peripheral blood were measured by flow cytometry. Hearts were isolated at either three or seven days after Sham or MI surgery and immediately placed in a solution of ice cold FACS buffer (5% FBS in PBS). The atria were removed and the ventricular tissue was minced and stored on ice. Minced samples were placed in 2 mL of digestion solution, comprised of 1.4 mg/mL of type II collagenase in HBSS, and incubated at 37°C for thirty minutes with rotation. The digested sample was then triturated forcefully and filtered through a 100 μm cell strainer. Resultant cells were washed in 50 mL of ice cold FACS buffer, centrifuged at 1500 rpm for 5 minutes, resuspended in FACS buffer and filtered through a 70 μm cell strainer into room temperature red blood cell lysis buffer (BioLegend). Similarly, peripheral blood was collected with a K-EDTA syringe by cardiac puncture and quickly diluted into room temperature red blood cell lysis buffer. After 5 minutes in lysis buffer, cells were washed in FACS buffer, centrifuged at 1500 rpm for 5 minutes, and counted to measure the total number of cells. Cells were then taken from each sample, suspended in DAPI (1:100,000; Thermo-Fisher Scientific) to label dead cells, and stained with conjugated antibodies for Ter-119 (1:100; violetFluor™ 450 clone TER-119; Tonbo Biosciences), CD45.2 (1:100; PerCP-Cy5.5 clone 104; Tonbo Biosciences),

CD31 (1:100; PE-Cy7 clone MEC13.3; BioLegend), CD11b (1:100; PE clone M1/70; eBioscience), CD206 (1:100; APC clone MR6F3; eBioscience), CD86 (1:100; FITC clone GL1; eBioscience), Gr-1 (1:100; FITC clone RB6-8C5; eBioscience). Staining for CDH11 was performed in a two-step process with an unconjugated primary antibody (1:100; clone 23C6; from M. Brenner (Chang et al. 2017)) followed by a PE secondary antibody (1:100; PE clone; RMG1-1; BioLegend). Note that antibodies specific for CD45.1 (1:100; PE clone A20; BD Biosciences) and CD45.2 (1:100; FITC clone 104; BD Biosciences) were used for assessment of bone marrow engraftment efficiency (**Figure S6**).

Gating based on size and shape (FSC and SSC), in addition to negative staining for DAPI and Ter-119, was used to identify viable single cells (**Figure S1**). Further gating based on fluorescence minus one (FMO) stained controls was used to identify the presence of distinct cell populations (**Figure S2**). In particular, we identified bone marrow derived cells (BMDC: $CD45^+$), cardiac endothelial cells (CEC: $CD45^-CD11b^-CD31^+$), and cardiac mesenchymal cells – primarily myofibroblasts – (CMC: $CD45^-CD11b^-CD31^-$). Within the BMDC population, we gated for bone marrow-derived pro-angiogenic cells (BMDPACs: $CD45^+CD11b^-CD31^+$), myeloid lineage cells ($CD45^+CD11b^+$), and non-myeloid lineage cells ($CD45^+CD11b^-CD31^-$). Note that non-myeloid lineage cells are predominately lymphocytes. Within the myeloid cell population, we identified various subpopulations including neutrophils ($CD45^+CD11b^+$Gr-$1/CD86^{hi}$), eosinophils ($CD45^+CD11b^+$Gr-$1/CD86^{lo}SSC^{hi}$), monocytes ($CD45^+CD11b^+$Gr-$1/CD86^{lo}SSC^{lo}$), and macrophages ($CD45^+CD11b^+$Gr-$1/CD86^{int}$) (Rose, Misharin, and Perlman 2012). Using this strategy, we further assessed macrophage polarization by gating for pro-inflammatory (M1-like) macrophages ($CD45^+CD11b^+$Gr-$1/CD86^{int}CD206^-$) and pro-resolving (M2-like) macrophages ($CD45^+CD11b^+$Gr-$1/CD86^{int}CD206^+$) (**Figure S1**). The neutrophil-to-lymphocyte ratio (NLR) was computed by dividing the number of positively identified neutrophils by the number of non-myeloid BMDCs in each sample (Chen et al. 2018).

Using the FMO control for CDH11 (**Figure S2**), this overall gating strategy was applied to 1) all live, single cells and 2) all live, $CDH11^+$ cells (**Figure S4C-D**). In this manner, we were able to compute the fraction of $CDH11^+$ cells within each cell population of interest identified in the heart (**Figure S3A** and **Figure 1**) and peripheral blood (**Figure S3B** and **FigureS5**). For studies involving SYN0012 and IgG2a treatments (**Figure 5** and **Figure S13**), the same gating strategy was used to identify cell populations of interest, although staining for CDH11 expression was not performed. Two-way ANOVA with Holms-Sidak's multiple comparison tests were used to determine significant changes in cell fraction between treatment groups and between days. The non-parametric Kruskal-Wallis test was used when the data being compared failed normality and equal variance tests.

Quantification of cardiac function and geometry by echocardiography

Ejection fraction (EF), left ventricular (LV) mass, and LV volume in both systole and diastole were measured from short axis cardiac M-Mode images captured on a Vevo 2100 small animal ultrasound system (VisualSonics). A minimum of six independent measures of LV diameter and wall thickness were used to calculate metrics of cardiac function and geometry for each mouse at each time point. Note that EF, LV mass and LV volume were calculated from the LV inner diameter at diastole and systole.

Echocardiographic measurements were made just prior to MI (baseline), as well as at days seven, 21, and 56 days after surgery. Mice with an EF reduced by less than 5% or greater than 70% were excluded from subsequent analyses. This ensured that all mice included in the study had consistently-sized (intermediate to large) infarcts which had not progressed to complete heart failure. In particular, for each group within the antibody treatment experiment, one mouse was excluded for a minor infarct and two were excluded with too large of an infarct. LV Mass measurements greater than 450 mg were excluded as outliers, likely caused by image artifacts due to fibrotic remodeling (only observed in

genotype comparison). Mice were euthanized by CO_2 inhalation in accordance with university guidelines at three, seven, 21 and 56 days after infarct for further processing.

Linear mixed-effect statistical analysis with the restricted maximum likelihood (REML) was performed to compare repeated measurements of echocardiological measurements in the same animals across times, treatments and genotypes. We considered the fixed effects (type III) for overall significant differences due to line/treatment group, day, and interaction between line and day. The post-hoc Holm-Sidak's method with an overall significance level of 0.05 was used to correct for multiple comparisons between days within a treatment group or genotype and to compare the effect of treatment within each day.

Bone marrow transplantation

Six week old male WT mice expressing the CD45.1 allele (B6.SJL-*Ptprc*^{a}*Pepc*^{b}/BoyJ; Jackson Laboratories) were lethally irradiated with a 10 Gy split dose from a Cs^{137} source (5 Gy in the morning followed by 5 Gy 4-6 hours later). Within 24 hours, age- and gender-matched *Cdh11*$^{+/+}$, *Cdh11*$^{+/-}$, and *Cdh11*$^{-/-}$ donors were euthanized and bone marrow was isolated from whole femurs and tibia. Donor bone marrow was delivered to irradiated recipients by retro-orbital injection (1×10^{6} cells in 100µL), and recipient mice were maintained on acidified water with antibiotics (neomycin and polymyxin B) for up to 2 weeks. Transplant efficiency was confirmed by flow cytometric analysis of isolated bone marrow showing simultaneous expression of the donor CD45.2 allele and absence of the original CD45.1 allele (**Figure S6**). To allow sufficient time for bone marrow reconstitution, mice received MI by permanent LAD ligation six weeks after transplantation.

Cryosectioning and quantitative histological analysis

Following euthanasia, hearts were dissected into PBS, weighed (**Figure S10A-B**), and then submerged briefly in a KCl solution to relax the CMs. Relaxed hearts were then bisected along the transverse plane (orthogonal to the long axis of the heart), embedded in OCT media, and frozen. Frozen blocks were subsequently cryosectioned into 10 μm sections, mounted onto glass slides, and stored at –20°C. A selection of the slides were stained using Masson's trichrome (Sigma), according to the manufacturer's instructions, in order to identify regions of healthy myocardium (red/pink), collagen/ECM deposition (blue), and cell nuclei (black) (**Figure S9**). Prior to staining, slides were brought to room temperature, OCT media was dissolved in PBS, and sections were fixed in Bouin's solution.

To quantify infarct morphology (length and thickness) from Masson's trichrome stained sections, a semi-automated image processing pipeline was developed (**Figure S9**). Briefly, non-uniformity in background illumination was corrected by bottom hat filtering prior to boundary detection. Using the detected boundaries, local ventricular wall thickness was computed using an Eulerian solution to a pair of linear partial differential equations over the histological domain (Yezzi and Prince 2003). By solving the Laplace equation for a given harmonic function f between the inner (ventricular lumen) and outer (myocardial wall) boundaries, the local thickness field was obtained. Correspondence trajectories along f between the inner and outer boundaries were used to subdivide histological sections into 40 circumferential partitions. (Rocha, Yezzi, and Prince 2007). Following partitioning, colorimetric segmentation in an HSL color space (Bersi et al. 2017) was performed in order to identify the area fractions of myocardium (red; H = 250° - 25°, S = 0.1 - 1.0, L = 0.1 - 0.93) and collagen (blue; H = 150° - 250°, S = 0.1 - 1.0, L = 0.1 - 0.93) within each partition. Based on the identified area fractions, locations of infarct borders were defined based on the inversion of area fractions (i.e., clockwise from red > blue to blue > red and vice-versa). Using this approach, the location and thickness profile of the infarcted regions were automatically identified. In cases of poor automatic detection, infarct borders were defined

manually. Finally, following identification of infarct borders, the ratio of infarct length to total circumferential length (in degrees) was used to estimate the percent circumference of the infarct region. Using the thickness profile between infarct borders, the average and standard deviation (i.e., thickness variation) were used to characterize infarct morphology (**Figure S10D-E**). Quantification was performed on 3 sections per heart separated by at least 300 μm.

Immunohistochemistry

Frozen slides were brought to room temperature, OCT media was dissolved in PBS, and tissue sections were fixed in 4% paraformaldehyde with 0.3% Triton-X for 10 min followed by blocking in 1% BSA in PBS for 1 hour. Tissue sections were then stained for either αSMA (Cy3; Sigma), CD31 (Biolegend: Alexa Fluor 594, clone 390), CD45 (FITC CD45.1; BD Pharmigen) or IL-6 (Abcam: clone 1A4). Sections stained with non-conjugated antibodies (IL-6) were incubated at a 1:100 dilution in 1% BSA overnight at 4°C. Sections were then rinsed with PBS and incubated with fluorescently tagged secondary antibodies (Goat anti Rabbit Alexa Fluor 647, Thermo) for 1 hour at a 1:300 dilution in 1% BSA. Sections stained with directly conjugated antibodies were incubated at a 1:100 dilution in 1% BSA for 1 hour at room temperature. Stained slides were mounted in ProLong Gold with DAPI to visualize cell nuclei and were imaged using an Olympus BX53 microscope equipped with a high resolution Qimaging Retiga 3000 camera. Muscularized vessels smaller than ~100 μm in diameter and myofibroblasts (defined as αSMA positive cells not colocalized with endothelial cells) present in one transverse section per heart collected from the center of the infarct zone were manually counted. The average number of muscularized vessels and myofibroblasts from hearts 21 days post-MI were compared with a Student's t-test.

Atomic force microscopy

Frozen slides were acclimated to room temperature, OCT media was dissolved in PBS, and tissue sections were blocked in 10% FBS for 20 minutes. Tissue sections were then stained for αSMA (Sigma) and a Hoechst nuclear stain (Invitrogen) for 20 minutes to allow for visualization of the infarct while scanning with the atomic force microscope (AFM). The Biocatalyst AFM developed by Bruker was used to measure tissue topography and stiffness within SYN0012 and IgG2a treated infarcts. The AFM probe was equipped with a blunted pyramidal tip specifically developed for soft biological samples (MLCT-Bio) and the peak force quantitative nanomechanical mapping scanning mode (PeakForce QNM) was used in order to provide robust measurements of topography and elastic modulus. Prior to scanning tissue samples, the system was calibrated on 40 kPa polyacrylamide gel standards and the spring constant and deflection sensitivity of the AFM probe was calculated. All measurements were made in PBS and were acquired from at least five separate 10x10 μm^2 areas from a minimum of two different sections per mouse (**Figure S8**). The median and interquartile range of stiffness from each scan were averaged for each mouse, and these measurements were averaged and compared by two-way ANOVA. The post-hoc Holm-Sidak's method with an overall significance level of 0.05 was used to account for multiple comparisons between treatment groups and different days.

Cell isolation and culture

To complement and inform our *in vivo* studies, cardiac fibroblasts (CFs) (Golden et al. 2012) and intraperitoneal macrophages (MΦs) were isolated from mice. CFs were isolated from *Cdh11*$^{+/+}$ and *Cdh11*$^{-/-}$ mice bred onto the *Immorto* mouse line, such that cells from littermate controls could be maintained in culture for longer. Briefly, hearts from eight week old mice were isolated, minced, and digested in a 2% collagenase solution supplemented with trypsin for the last 10 minutes of a 40 minute

digest. CFs were then rinsed with PBS, transferred to gelatin coated plates, and cultured in DMEM supplemented with 10% FBS, 1% penicillin/strep, and interferon gamma at 33°C in order to maintain the immortalized phenotype. Prior to experimental use, cells were replated in DMEM supplemented with 10% FBS and 1% penicillin/strep and grown at 37°C for 48 hours to deactivate the immortalized gene.

MΦ exfiltration was stimulated by intraperitoneal (IP) injection of 1mL of 4% thioglycollate media into C57BL/6 mice. After 72 hours, mice were sacrificed and the intraperitoneal cavity was flushed with 10 mLs of cold RPMI media to collect the cells. After washing in cold PBS, cells were plated in RPMI media supplemented with 10% FBS on tissue culture plastic and allowed to adhere for 1 hour. Following previous reports, non-adherent cells were then rinsed away and all remaining cells were taken to be macrophages (Zhang, Goncalves, and Mosser 2008).

Gel contraction assay

Isolated CFs (WT and *Cdh11*$^{-/-}$) were diluted in a 1.28 mg/mL collagen solution derived from PureCol (Advanced Biomatrix) to a final concentration of 250,000 cells/mL and were poured into a Teflon ring in a suspension well. After polymerizing for 1 hour, DMEM supplemented with 10% FBS and 1% penicillin/strep was added to flood the well and release the collagen gel from both the bottom of the well and the Teflon ring. Gels were imaged immediately after release and at multiple times over the next 48 hours. At each time point, gel areas were measured in ImageJ and normalized to the original gel area. For comparison of the impact of IgG2a and SYN0012 treatment, antibody was added to the cell/gel mixture at a final concentration of 20 μg/ml prior to pouring; media added to the well also contained 10 μg/ml of antibody (**Figure S11**).

qPCR

For assessment of *in vivo* transcription of specific pro-fibrotic and inflammatory genes of interest, hearts were isolated under RNAse-free conditions and immediately flash frozen. For isolation of mRNA, samples were subsequently thawed and lysed in TRIZOL with chloroform induced phase separation according to manufacturer's instructions. cDNA was synthesized using the Superscript IV kit (Invitrogen) using 500 ng of mRNA. Real time qPCR was used to amplify targets from the cDNA using a SYBR green master mix (BIO-RAD) and specific primer sets (**Table S1**). The BIO-RAD CFX96 C1000 system was used to quantify gene transcription in each sample, relative to *Gapdh*. For all of the *in vivo* transcription levels, post-MI samples were normalized to the average of all three and seven day Sham values (**Figure S14**).

Two-way ANOVAs were used to compare the relative transcription of targets of interests in IgG2a- and SYN0012-treated mice receiving MI and Sham animals that received neither MI nor antibody treatment at day three and day seven. An additional one-way ANOVA was run to compare the transcription levels of IgG2a and SYN0012 treated animals at 21 days after infarct and the average transcription of Sham animals. Two-way ANOVAs with Holm-Sidak's multiple comparison tests were also used to compare IgG2a and SYN0012 samples across all time points.

Table S1 qPCR primers

Target	Forward	Reverse
Gapdh	ATGACAATGAATACGGCTACAG	TCTCTTGCTCAGTGTCCTTG
Ctnt	AGGAGCTGATTTCCCTCAAAG	TTTCCTTCTCCCGCTCATTG
Cdh11, exon12	TCACTATCAAAGTCTGTGGCTG	CAAACAGCACAACGATGACC
Il6	CAAAGCCAGAGTCCTTCAGAG	GTCCTTAGCCACTCCTTCTG

F4/80	ACCACAATACCTACATGCACC	AAGCAGGCGAGGAAAAGATAG
Il1β	TCCTGTGTAATGAAAGACGGC	ACTCCACTTTGCTCTTGACTTC
Tnfα	AGACCCTCACACTCAGATCA	TGTCTTTGAGATCCATGCCG
Mmp3	CAGGAAGATAGCTGAGGACTTTC	GGTCAAATTCCAACTGCGAAG
Mmp13	GATTATCCCCGCCTCATAGAAG	TCTCACAATGCGATTACTCCAG
Tgfβ1	CCTGGGTTGGAAGTGGATC	TTGGTTGTAGAGGGCAAGG
αsma	GAGAAGCCCAGCCAGTCG	CTCTTGCTCTGGGCTTCA
Col1a1	CACCCTCAAGAGCCTGAGTC	GTTCGGGCTGATGTACCAGT
Fgf2	GGAGTTGTGTCTATCAAGGGAG	TGCCCAGTTCGTTTCAGTG
Vegfa1	AAAGCCAGCACATAGGAGAG	CGAGTCTGTGTTTTTGCAGG
Mrc1	ATGGATGTTGATGGCTACTGG	TTCTGACTCTGGACACTTGC
Cd14	CCTTTCTCGGAGCCTATCTG	CAACTTTCCTCGTCTAGCTCG
Arg1	AAGAATGGAAGAGTCAGTGTGG	GGGAGTGTTGATGTCAGTGTG

Quantification of IL-6 production by indirect ELISA

CFs were plated in each well of a 12 well plate (50,000 CFs/well) and allowed to adhere for 20 min prior to exposure to media containing between 0 and 50,000 MΦs. Cell suspensions were diluted to a final volume of 1.3 mL per well. We tested the interaction of cells (including MΦs alone) without antibody treatment, and then specifically compared CFs and a range of co-culture with IgG2a or SYN0012. For antibody treatments, samples were incubated with antibody (10 μg/ml) for 15 minutes before plating. After 48 hours in culture, conditioned media was removed from each well and IL-6 secretion was measured with a DuoSet mouse IL-6 ELISA (R&D Systems). After boiling, 100 μl of each sample was added in duplicate and compared against a provided standard (**Figure 7A-B**). Cells from these co-cultures were also lysed in TRIZOL for isolation of mRNA, cDNA synthesis, and analysis of transcription of specific gene targets by qPCR, as described above (**Figure 7C-E** and **Figure S15**).

One-way ANOVA with a post-hoc Holm-Sidak test to account for multiple comparisons was used to test for differences in expression of IL-6 and transcription of *MMP13* by untreated CFs with different CF:MΦ ratios. Two-way ANOVAs were run to compare the effect of increasing numbers of MΦs and treatment with either IgG2a or SYN0012 on IL-6 expression and gene transcription. The post-hoc Holm-Sidak method with an overall significance level of 0.05 was used to account for multiple comparisons within cell types and treatment groups.

References

Bersi, M R, R Khosravi, A J Wujciak, D G Harrison, and J D Humphrey. 2017. “Differential Cell-Matrix Mechanoadaptations and Inflammation Drive Regional Propensities to Aortic Fibrosis, Aneurysm or Dissection in Hypertension.” *Journal of the Royal Society, Interface* 14 (136): 1–31. https://doi.org/10.1098/rsif.2017.0327.

Chang, Sook Kyung, Ayano C. Kohlgruber, Fumitaka Mizoguchi, Xavier Michelet, Benjamin J. Wolf, Kevin Wei, Pui Y. Lee, et al. 2017. “Stromal Cell Cadherin-11 Regulates Adipose Tissue Inflammation and Diabetes.” *Journal of Clinical Investigation* 127 (9): 3300–3312. https://doi.org/10.1172/JCI86881.

Chen, Chen, Bai Lin Cong, Min Wang, Muhammad Abdullah, Xiao Long Wang, Yin Hua Zhang, Shun Ji Xu, and Lan Cui. 2018. “Neutrophil to Lymphocyte Ratio as a Predictor of Myocardial Damage and Cardiac Dysfunction in Acute Coronary Syndrome Patients.” *Integrative Medicine Research* 7 (2): 192–99. https://doi.org/10.1016/j.imr.2018.02.006.

Gao, Erhe, Yong Hong Lei, Xiying Shang, Z. Maggie Huang, Lin Zuo, Matthieu Boucher, Qian Fan, J. Kurt Chuprun, Xin L. Ma, and Walter J. Koch. 2010. “A Novel and Efficient Model of Coronary Artery Ligation and Myocardial Infarction in the Mouse.” *Circulation Research* 107 (12): 1445–53. https://doi.org/10.1161/CIRCRESAHA.110.223925.

Golden, H B, D Gollapudi, F Gerilechaogetu, J Li, R J Cristales, X Peng, and D E Dostal. 2012. “Isolation of Cardiac Myocytes and Fibroblasts from Neonatal Rat Pups.” *Methods Mol Biol* 843: 205–14. https://doi.org/10.1007/978-1-61779-523-7_20.

O’Connell, Timothy D., Manoj C. Rodrigo, and Paul C. Simpson. 2007. “Isolation and Culture of Adult Mouse Cardiac Myocytes.” In *Cardiovascular Proteomics*, 271–96. New Jersey: Humana Press. https://doi.org/10.1385/1-59745-214-9:271.

Rocha, Kelvin R., Anthony J. Yezzi, and Jerry L. Prince. 2007. “A Hybrid Eulerian-Lagrangian Approach for Thickness, Correspondence, and Gridding of Annular Tissues.” *IEEE Transactions on Image Processing* 16 (3): 636–48. https://doi.org/10.1109/TIP.2007.891072.

Rose, Shawn, Alexander Misharin, and Harris Perlman. 2012. “A Novel Ly6C/Ly6G-Based Strategy to Analyze the Mouse Splenic Myeloid Compartment.” *Cytometry Part A* 81A (4): 343–50. https://doi.org/10.1002/cyto.a.22012.

Yezzi, Anthony J, and Jerry L Prince. 2003. “An Eulerian PDE Approach for Computing Tissue Thickness.” *IEEE Transactions on Medical Imaging* 22 (10): 1332–39. https://doi.org/10.1109/TMI.2003.817775.

Zhang, X, R Goncalves, and D M Mosser. 2008. “The Isolation and Characterization of Murine Macrophages.” *Curr Protoc Immunol* Chapter 14: Unit 14 1. https://doi.org/10.1002/0471142735.im1401s83.

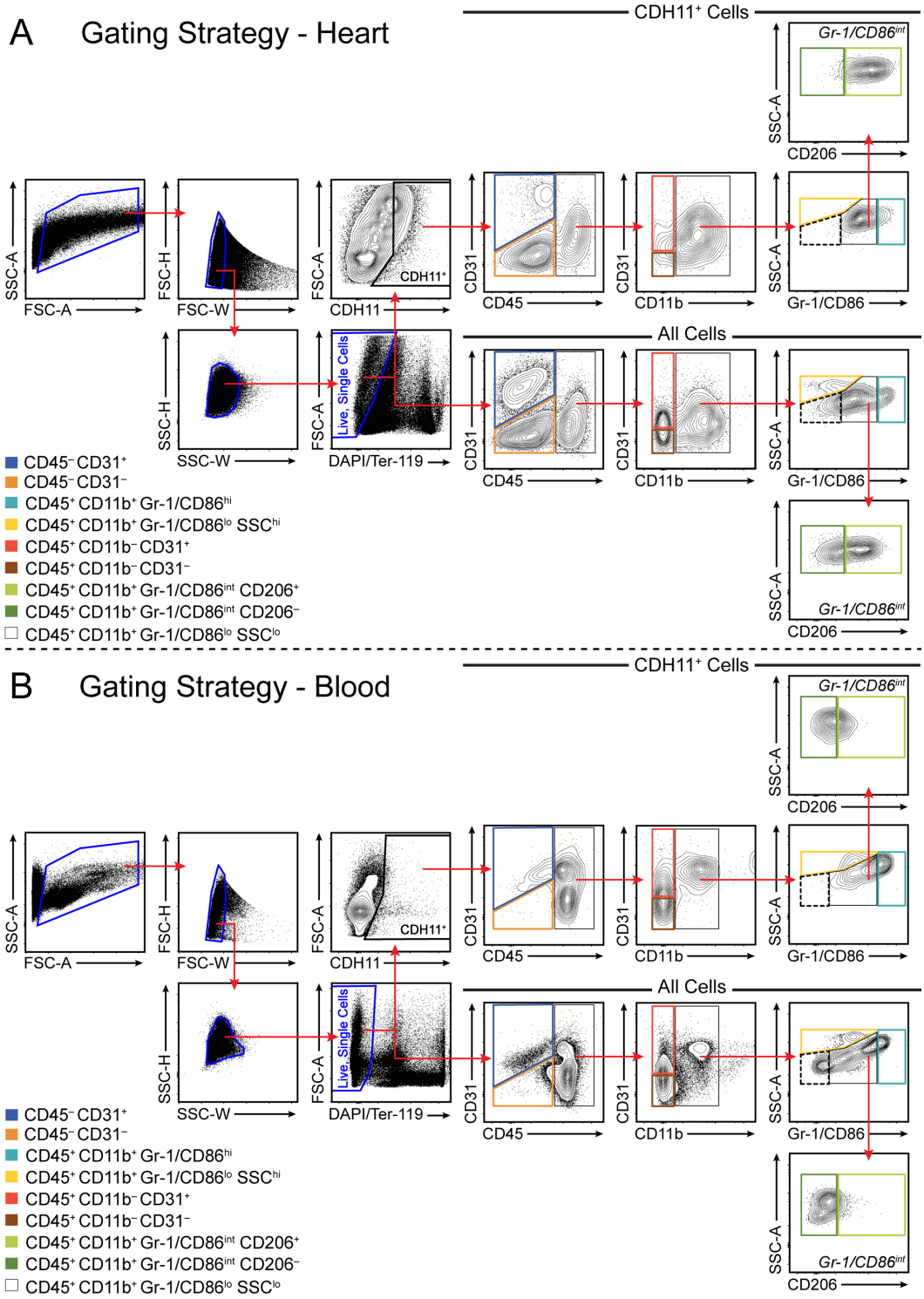

Figure S1. Flow cytometry gating strategy. Live single cells were identified from all measured events in the heart (**A**) and blood (**B**). Cells were gated into cardiac endothelial cells (blue), cardiac mesenchymal cells (orange), and bone-marrow derived cells (BMDCs). BMDCs were further gated into bone marrow-derived proangiogenic cells (red), non-myeloid lineage BMDCs (brown; lymphocytes), and myeloid lineage cells including neutrophils (light blue), eosinophils (yellow), monocytes (white/dashed) and macrophages. Macrophage polarization was assessed by defining M1-like macrophages (dark green) and M2-like macrophages (light green). Gating was applied to all events (bottom rows) and CDH11$^+$ cells (top rows) and is shown for representative samples at seven days after infarct.

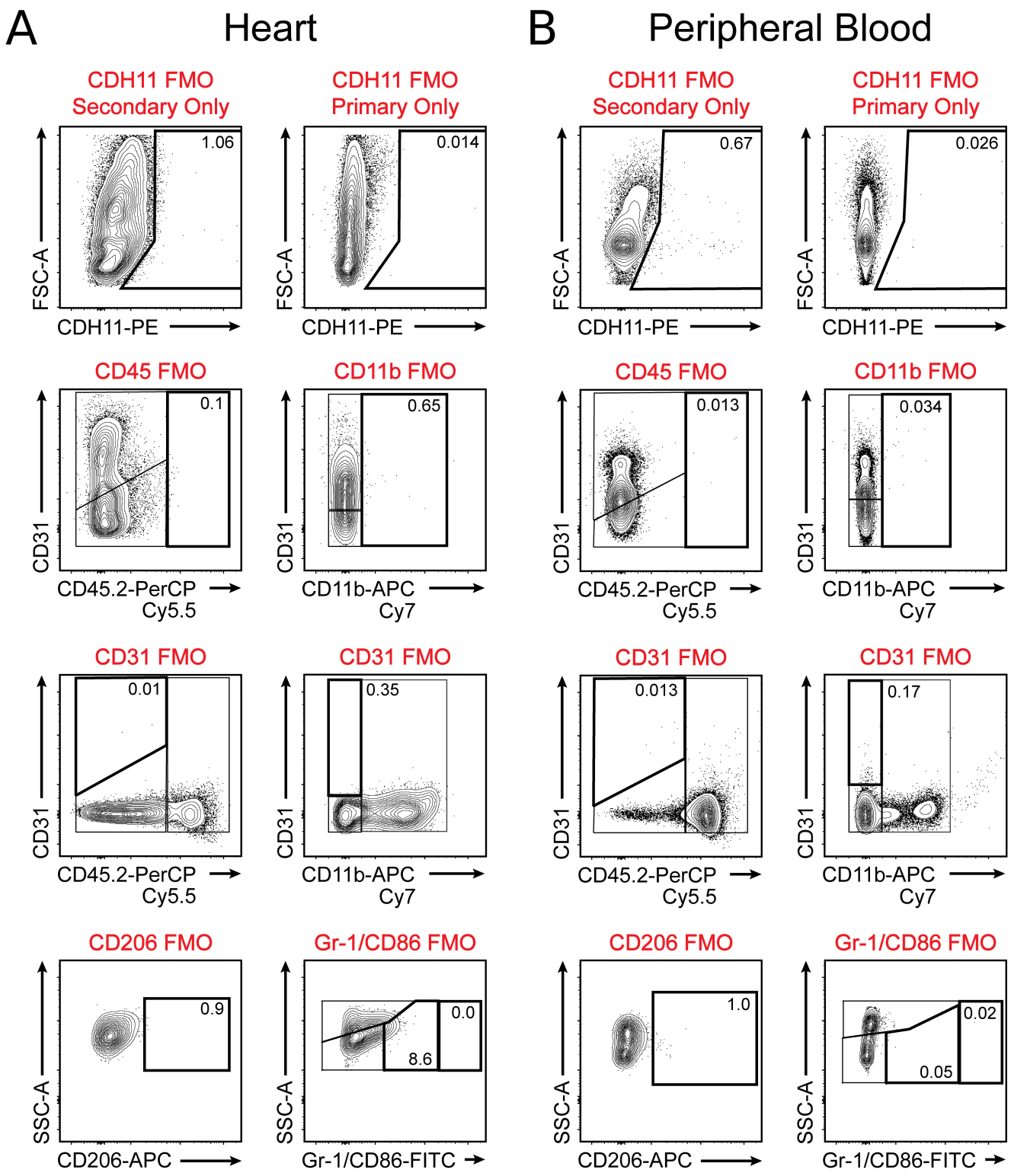

Figure S2. Fluorescence minus one (FMO) controls for flow cytometry analysis. FMO controls for each antibody used in the flow cytometric analyses indicates the placement of gates defining each of the primary cell populations in the heart (**A**) and peripheral blood (**B**). Inset numbers show the percent of parent population events that fall within each gate.

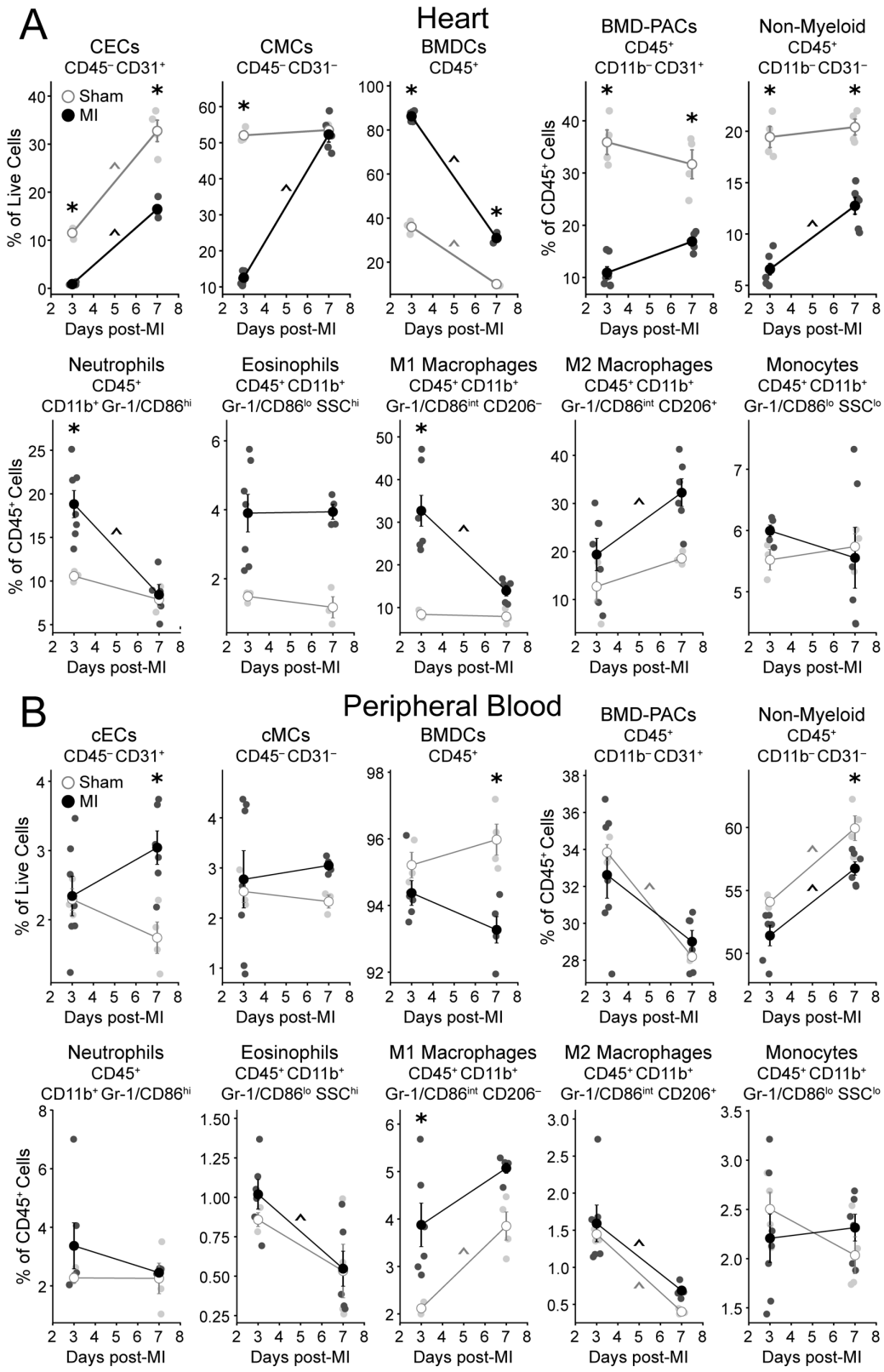

Figure S3. Changes in resident and bone marrow derived cell expression after MI. Flow cytometric analysis allows for quantification of each of the identified non-cardiomyocyte cell populations as a percentage of all live single cell events in the heart (**A**) and peripheral blood (**B**) after MI. * $p < 0.05$ between Sham and MI at the same time, ^ $p < 0.05$ over time; n = 3-7 per group.

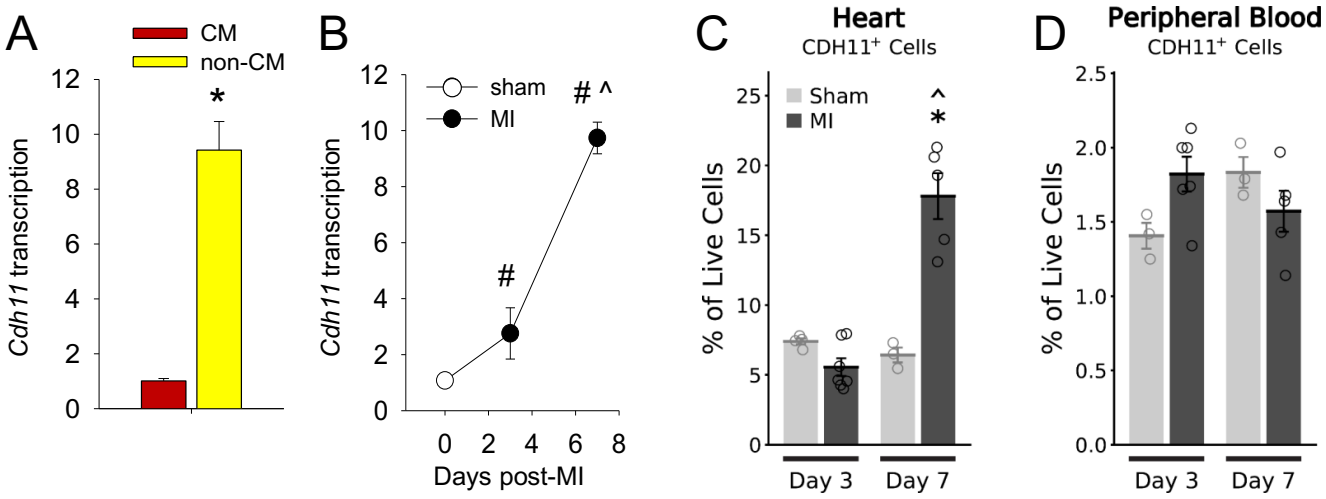

Figure S4. CDH11 expression is increased in the heart post-MI. Transcription of *Cdh11* occurs primarily in non-CM cells (**A**) and increases up to maximal expression (~10-fold higher than Sham) at day seven after MI (**B**). Flow cytometric analysis allows for quantification of CDH11$^+$ cells as a percentage of all live single cell events, in the heart (**C**) and peripheral blood (**D**) after MI. For **A-B**: * $p < 0.05$ between cell types, # $p < 0.05$ relative to Sham, ^ $p < 0.05$ relative to previous time point; For **C-D**: * $p < 0.05$ between Sham and MI at the same time, ^ $p < 0.05$ over time; n = 3-7 per group.

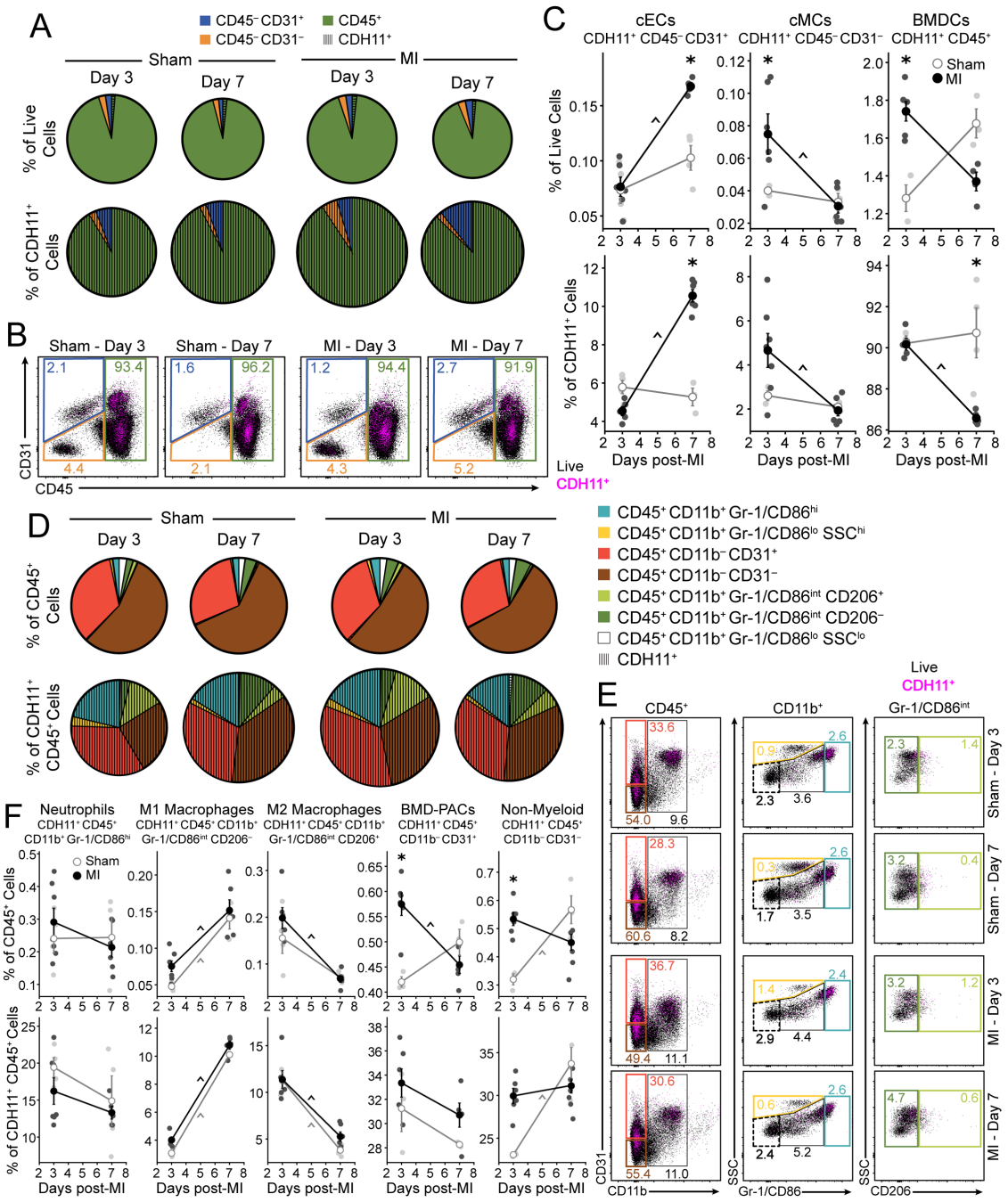

Figure S5. CDH11 expression in the blood is largely unaffected post-MI. Flow cytometric analysis reveals that circulating endothelial (cEC), mesenchymal (cMC), and bone marrow derived (BMDC) cell populations have minimal baseline CDH11 expression and are largely unaffected post-MI (hatched wedges). Pie chart radii (**A**) are scaled by either the number of live single cells (top row) or the number of CDH11$^+$ cells (bottom row) relative to that in Sham hearts at day three. Representative dot plots (**B**) show CDH11 expression (magenta) within each cell population (colored gates). CDH11$^+$ cells (**C**) within each population are shown as either a percentage of live cells (top row) or of all CDH11$^+$ cells. While CDH11 expression was low (<2% of total cells), the percent of CDH11$^+$ cells that are cECs is increased and that are BMDCs is decreased, relative to Sham, at day seven post-MI. BMDC subpopulations (**D**) revealed little CDH11 expression with little difference between Sham and MI. Representative dot plots (**E**) show CDH11 expression (magenta) within each subpopulation (colored gates). Though CDH11 expression was low in each BMDC subpopulation (<1% of CD45$^+$ cells), there was an increase in CDH11$^+$ BMD-PACs and CDH11$^+$ non-myeloid BMDCs at three days post-MI, with non-myeloid BMDCs comprising significantly more of all CDH11$^+$ BMDCs than Sham at day three. Percentages of each population, relative to all live cell events, are denoted within colored gates. * $p < 0.05$ between Sham and MI at the same time, ^ $p < 0.05$ over time; n = 3-7 per group.

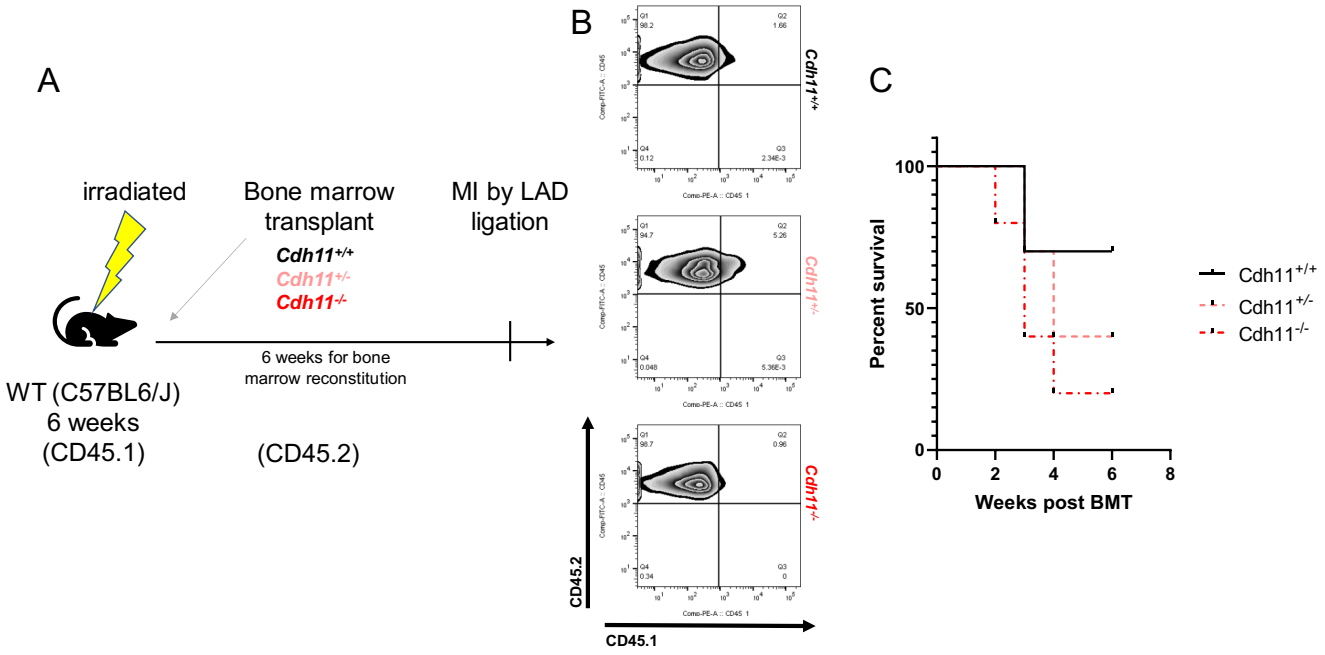

Figure S6: Experimental protocol for bone marrow transplantation. Schematic of experimental protocol for bone marrow transplantation from *Cdh11* transgenic donors (CD45.2) into lethally irradiated C57BL6/J recipients (CD45.1; B6.SJL-*Ptprc*^{a}*Pepc*^{b}/BoyJ) (**A**). Flow cytometry of CD45.1 and CD45.2 expression in the bone marrow after 6 weeks of reconstitution was used to confirm successful bone marrow transplantation (**B**). Despite successful transplantation, fewer mice with *Cdh11* transgenic bone marrow (e.g., *Cdh11*$^{+/-}$ and *Cdh11*$^{-/-}$) survived to the point of complete bone marrow reconstitution and the subsequent MI surgery (**C**).

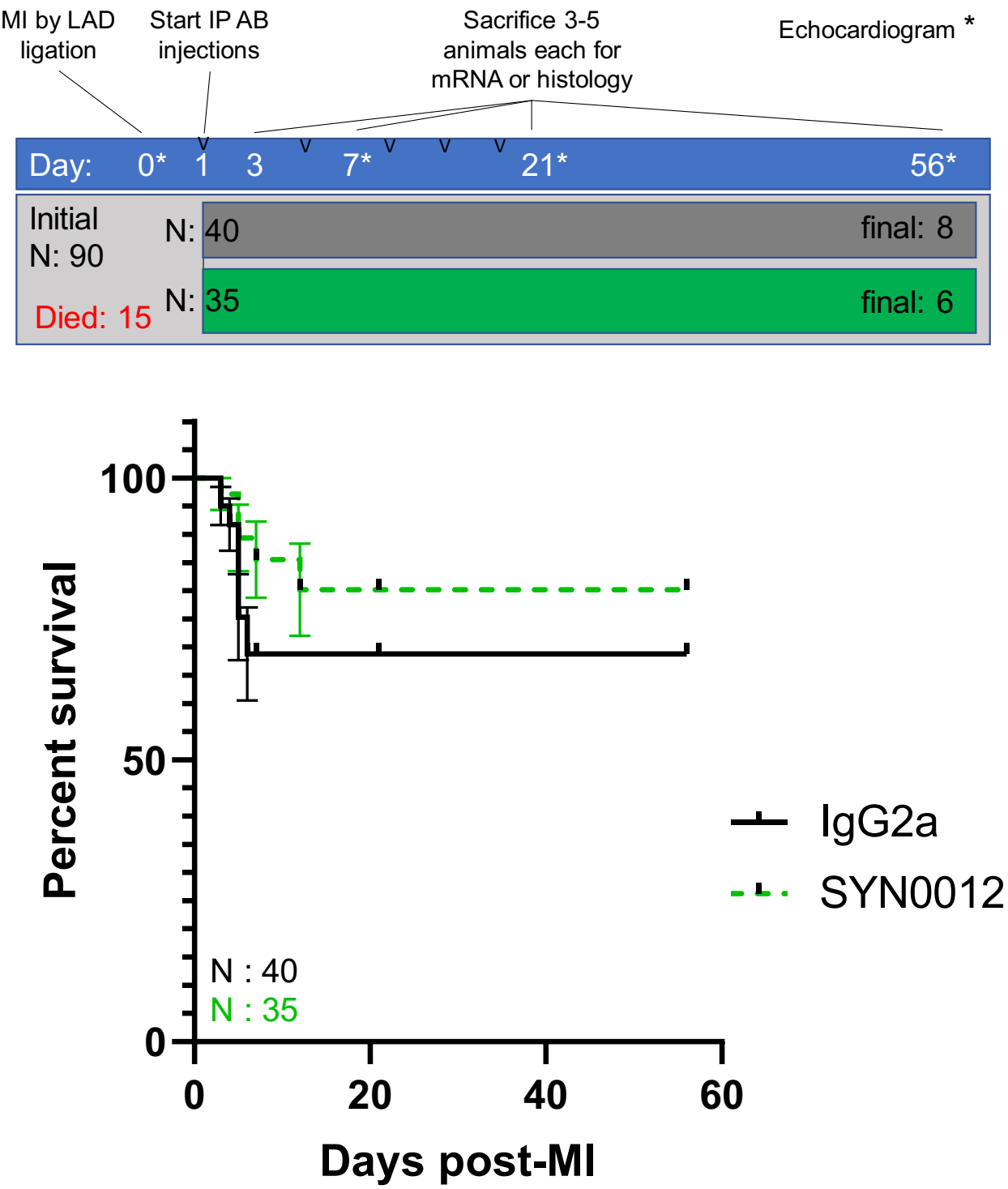

Figure S7: CDH11 blockade improves survival after MI. Experimental time course of antibody treatment, with injection days marked with 'v', and days of echocardiogram marked with '*'. Following MI, fewer animals receiving SYN0012 treatment died than those receiving IgG2a. Error bars represent standard error (SE).Though survival was improved, the findings were not statistically significant with a value of $p = 0.20$ following a Gehan-Breslow-Wilcoxon test.

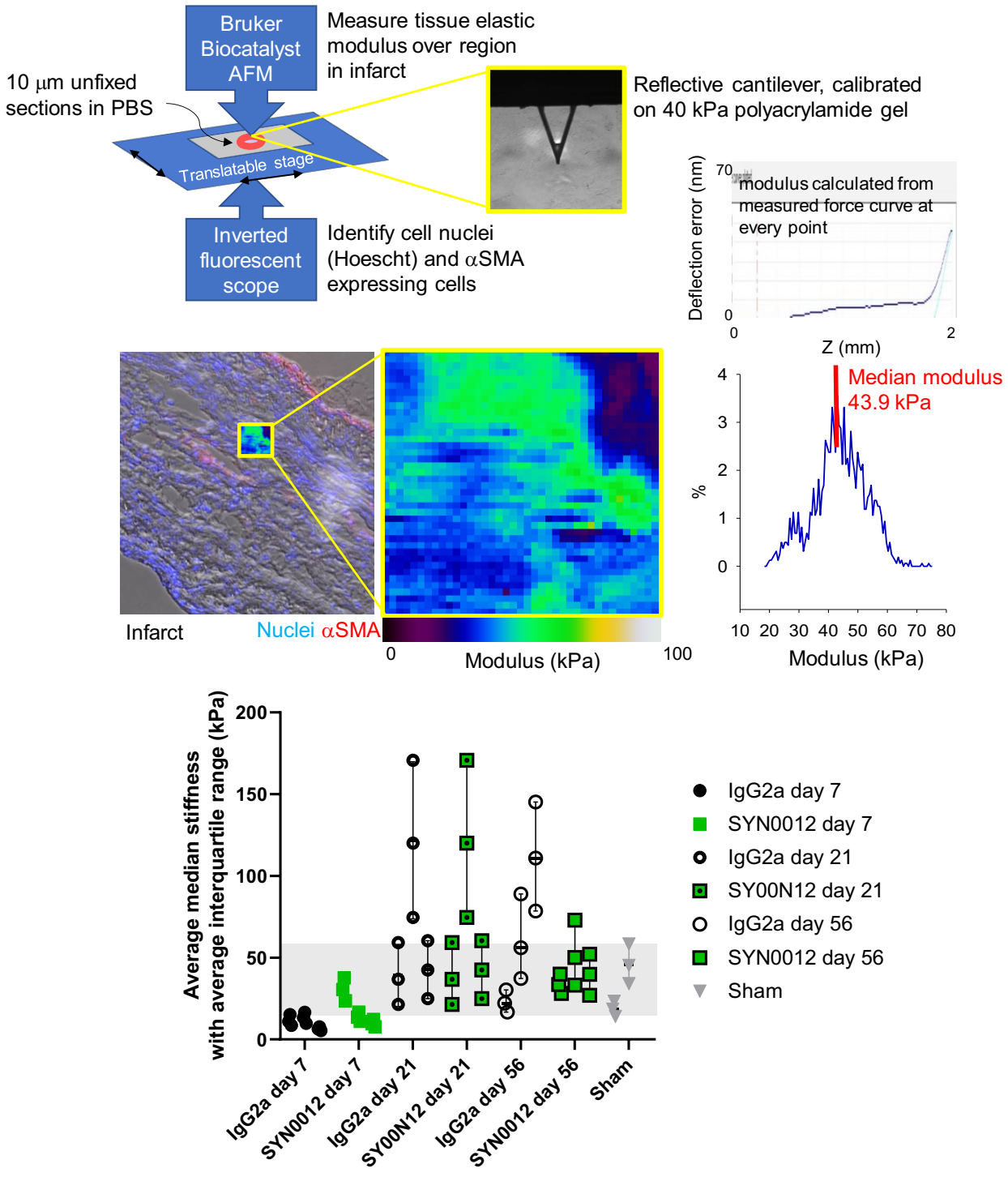

Figure S8: Atomic force microscopy and stiffness measurement pipeline. Schematic of atomic force microscopy (AFM) and fluorescent microscope arrangement, with a callout image of the pyramidal probe cantilever (top panel; yellow). A typical indentation curve from PeakForce QNM mode is also shown (top right). Representative area scan from 10x10μm^2 of infarcted tissue is shown with fluorescently labeled nuclei (blue) and αSMA$^+$ cells (red). Inset shows representative stiffness (modulus) colormap (middle let panel) and a corresponding histogram shows the distribution and median of measured moduli (middle right panel). For each mouse, tissue sections were analyzed by AFM and the average median stiffness and interquartile range was averaged from 6-8 scans per mouse.

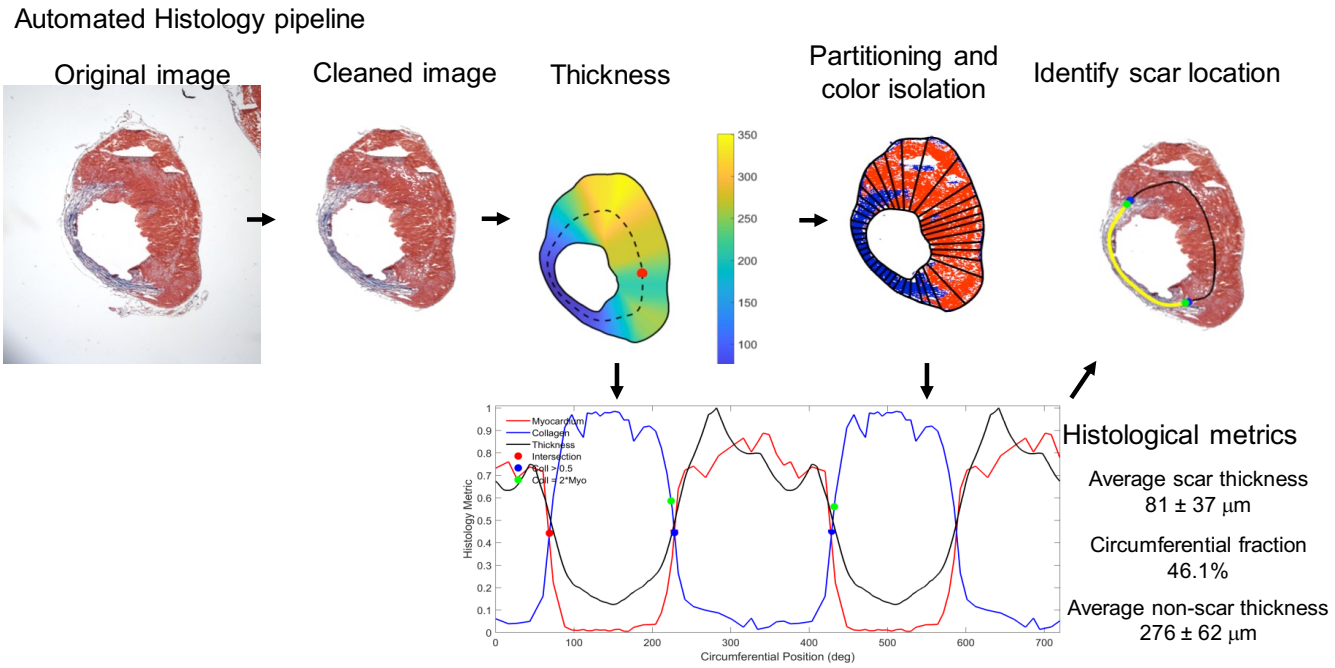

Figure S9: Semi-automatic histological image analysis pipeline. Masson's trichrome stained short-axis sections of infarcted hearts were analyzed in order to quantify infarct morphology such as infarct length as a circumferential percentage and average infarct thickness. Following background removal, thickness between the identified inner and outer boundaries is computed. A total of 40 circumferential partitions are defined, and colorimetric segmentation of red and blue pixels is performed (shown as pseudo-colored image). Infarct borders are then defined based on intersections between red/blue area fractions (bottom panel); infarct and non-infarct morphology (length, thickness, variance, etc.) is computed following semi-automatic identification of infarct borders.

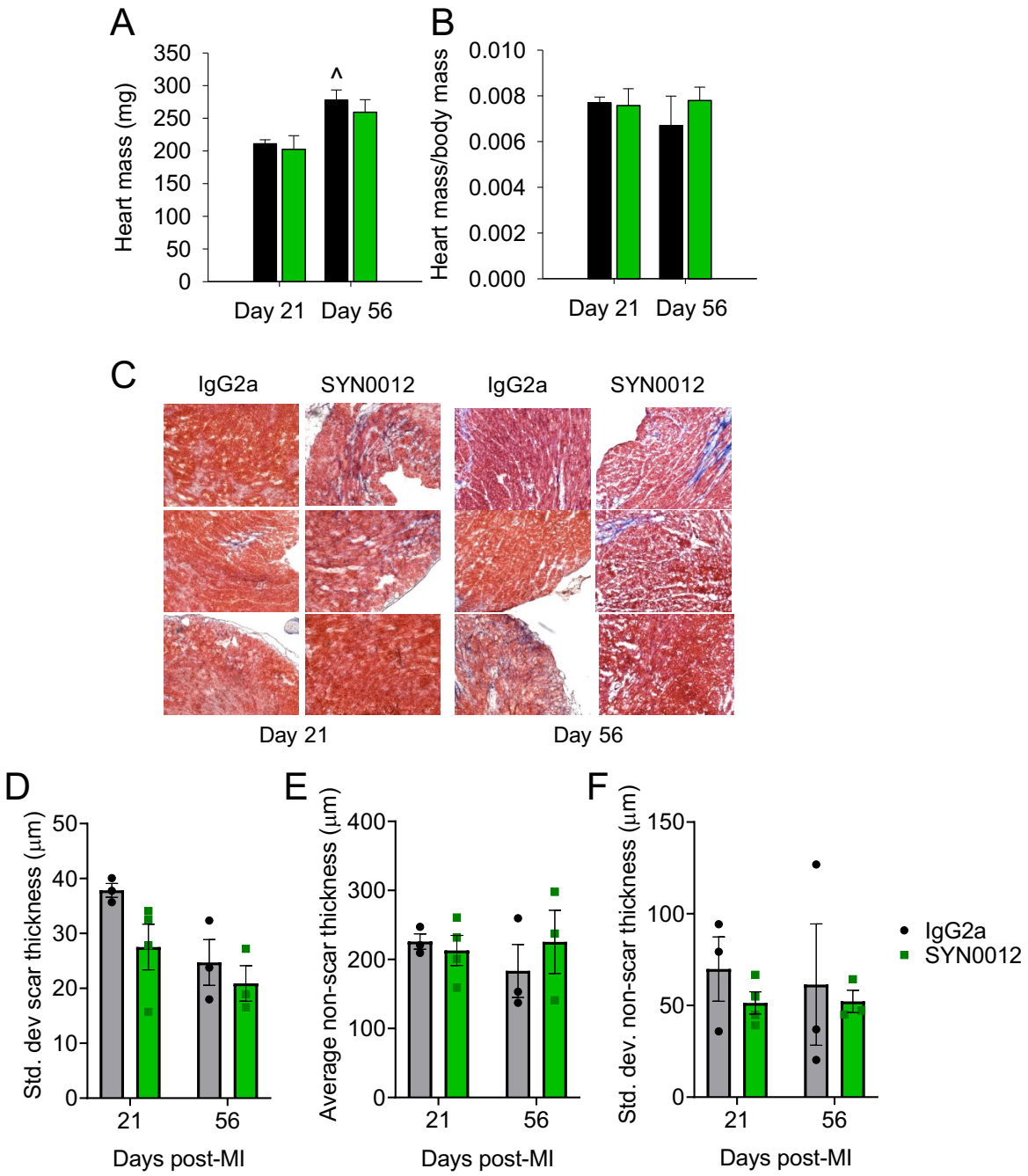

Figure S10. CDH11 blockade has little effect on cardiac hypertrophy and interstitial fibrosis. Quantification of heart mass (**A**) and heart to body mass ratio (**B**) revealed minimal differences aside from a significant increase in heart mass from 21 to 56 days in IgG2a-treated hearts that was not observed with SYN0012 treatment. Visual inspection of Masson's Trichrome staining of distant regions of the myocardium (three hearts per group shown) revealed no difference in remote interstitial fibrosis in each of the three (**C**) and there was also no significant difference in the measured standard deviation of the scar thickness and average and standard deviation of the non-scar thickness (**D-F**) at days 21 and 56 between treatments. ^ $p < 0.05$ between timepoints; $n \geq 3$ per group.

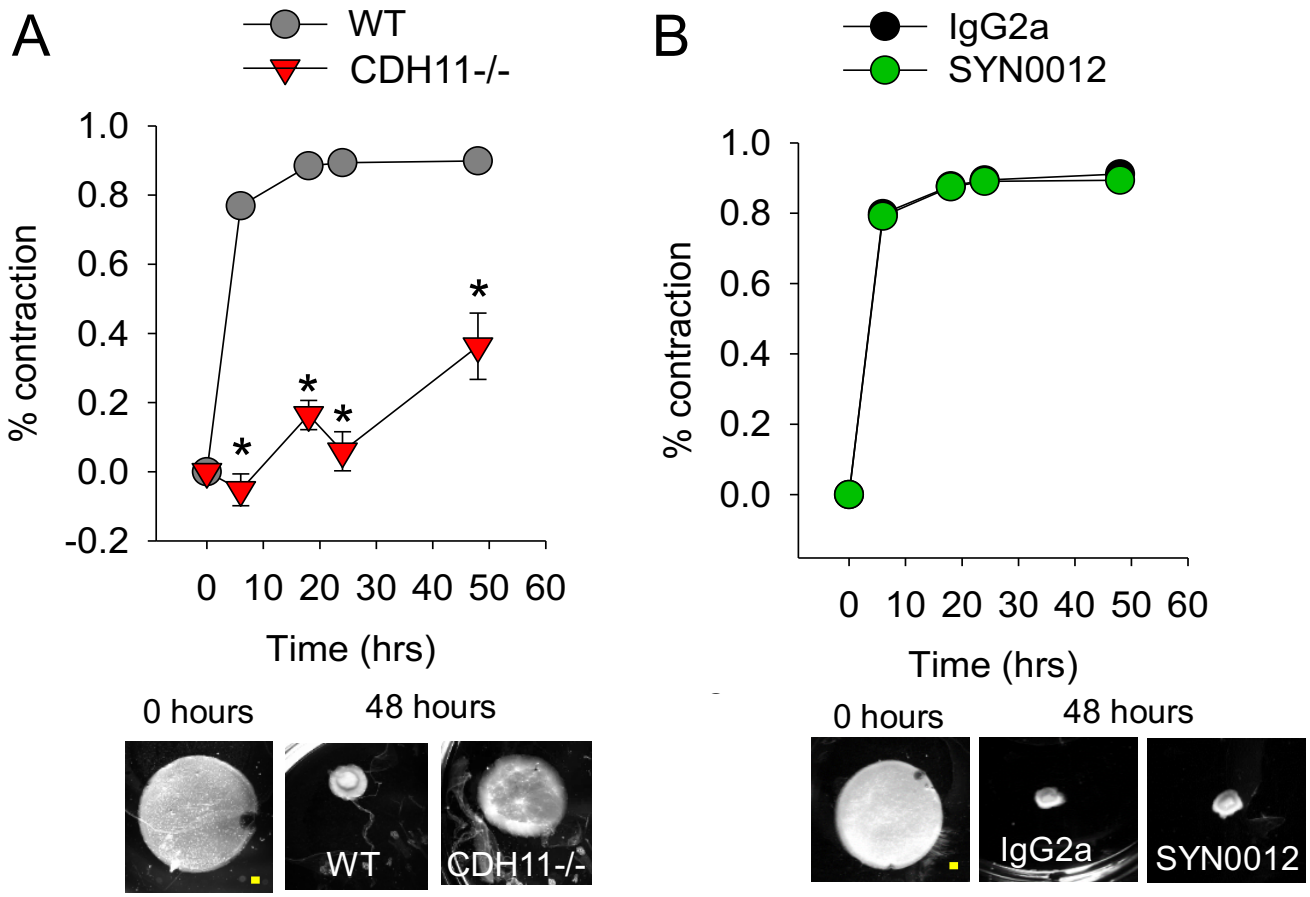

Figure S11: CDH11 modulates cardiac fibroblast contraction. Cardiac fibroblasts (CFs) isolated from *Cdh11*$^{-/-}$ mice exhibit a reduction in contractile ability relative to *Cdh11*$^{+/+}$ control CFs, as shown by a reduction in collagen gel contraction (**A**). Pharmacologic targeting of CDH11 in WT (C57BL6/J) CFs with SYN0012 treatment does not affect CF contractility and gel contraction (**B**). Yellow scale bar represents 1 mm. * $p < 0.05$ between groups at the same time; n = 3 per group.

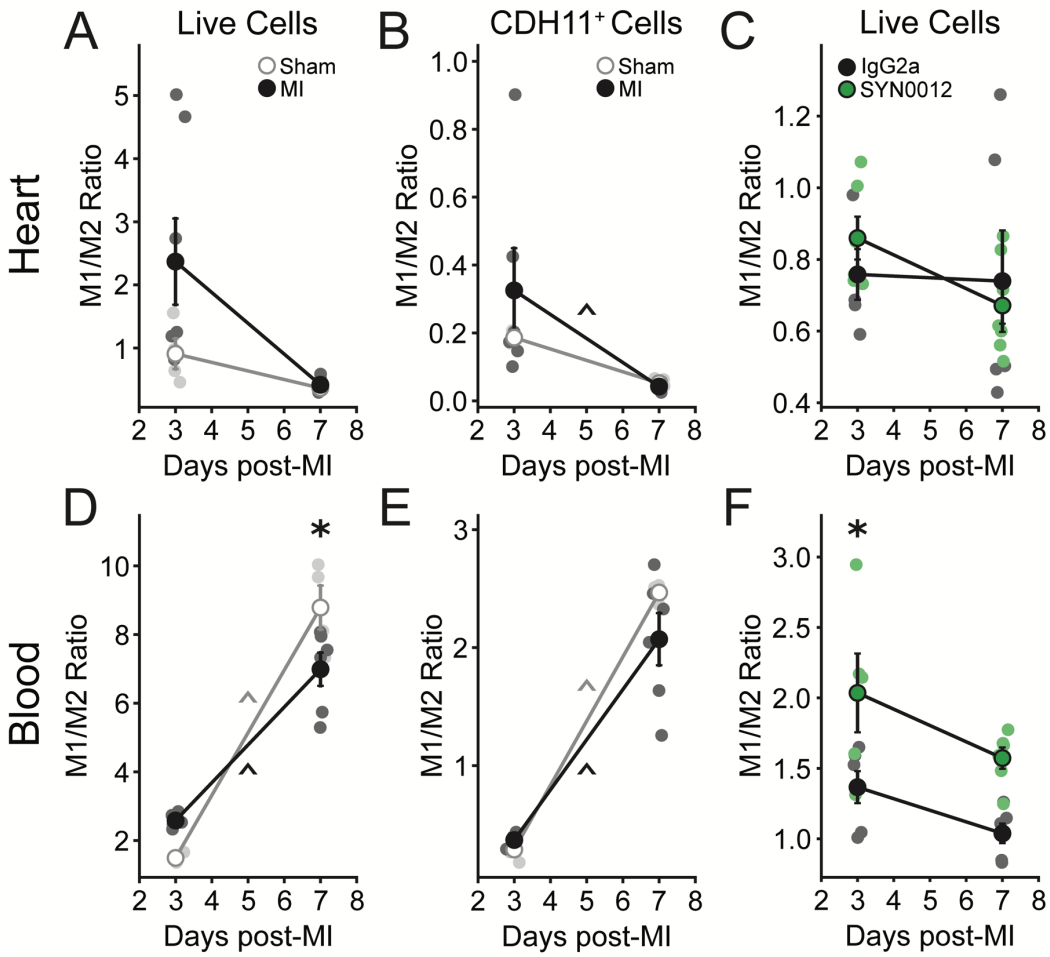

Figure S12. Ratios of macrophage polarization are affected by MI. Flow cytometric analysis reveals that the ratio of M1:M2-like macrophages in the heart was increased, though not significantly different, relative to Sham at day three when calculated as a percentage of all live cells (**A**) and all CDH11$^+$ cells (**B**). Cardiac M1:M2-like ratios were not different between IgG2a and SYN0012 treatments (**C**). M1:M2-like ratios based on all live cells in the peripheral blood significantly increased in Sham animals between day three and seven, and was larger than MI samples at day seven (**D**), but was not significantly affected in the CDH11$^+$ populations (**E**). SYN0012 treatment resulted in a higher M1:M2-like macrophage ratio that IgG2a after three days (**F**) which may suggest that CDH11 blockade alters macrophage recruitment to the heart after MI. * $p < 0.05$ between either Sham and MI or antibody treatments at the same time, ^ $p < 0.05$ over time; n = 3-7 per group.

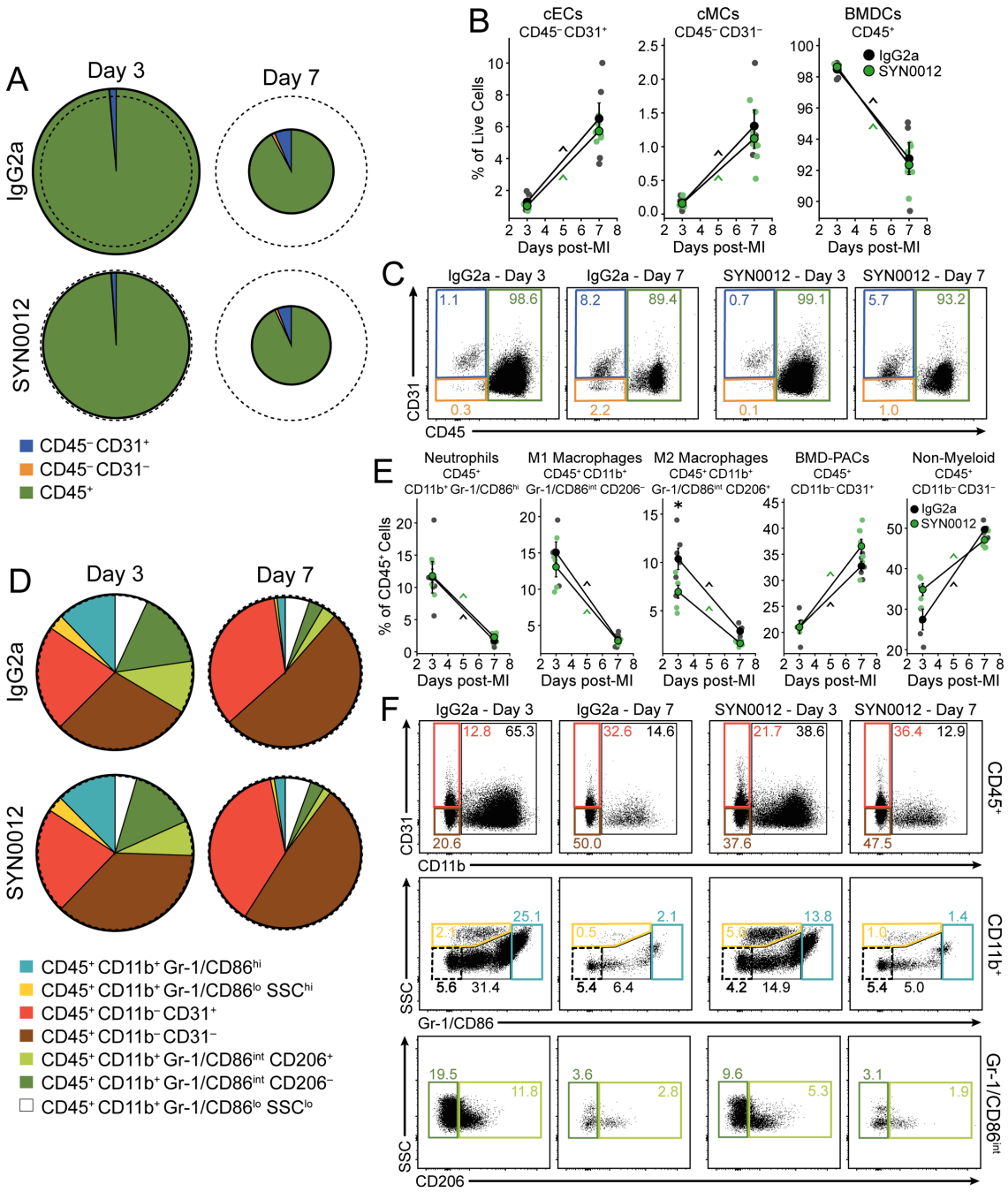

Figure S13. CDH11 blockade has little effect on circulating cell populations post-MI. Flow cytometric analysis reveals that CDH11 blockade by SYN0012 does not alter the percentages of circulating endothelial (cEC), mesenchymal (cMC), and bone marrow derived (BMDC) cells in the blood post-MI, relative to IgG2a, but differences are seen over time (**A-B**). Pie chart radii are scaled by the number of live single cells for each treatment and time, relative to Sham blood samples at day three (denoted by dotted circles). Representative dot plots (**C**) show changes in expression of each cell population (colored gates). Separation of BMDC subpopulations (**D**) revealed that SYN0012 significantly decreases circulating M2-like macrophages and shows a trend toward increasing non-myeloid BMDCs (lymphocytes) at day three (**E**). Differences were observed over time in all populations. Representative dot plots (**F**) show changes in expression of each BMDC subpopulation (colored gates). Percentages of each population, relative to all live cell events, are denoted within colored gates. * $p < 0.05$ between treatments at the same time, ^ $p < 0.05$ over time; n = 3-7 per group.

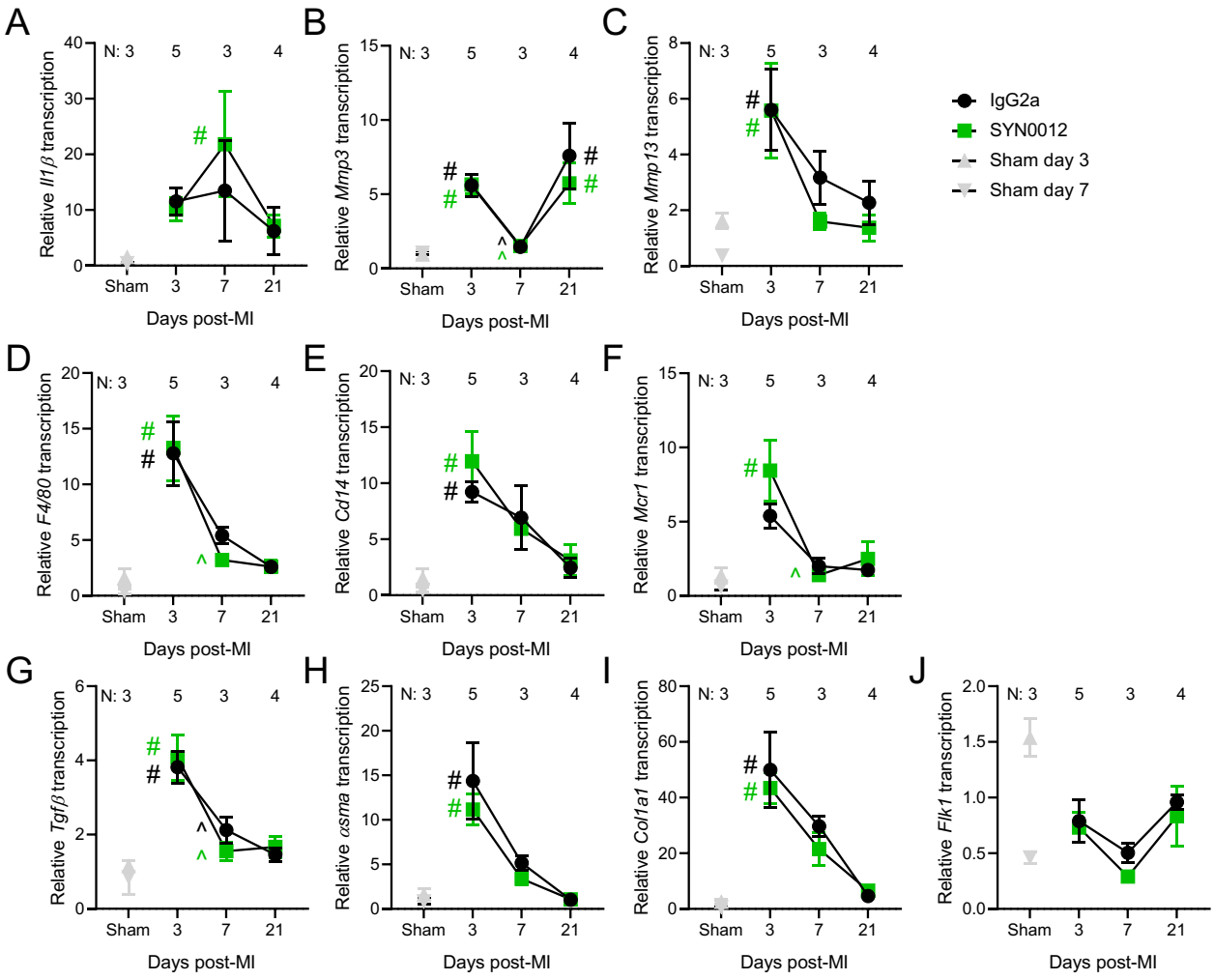

Figure S14: MI induces transcriptional changes in pro-inflammatory and pro-fibrotic genes. qPCR was used to characterize the time-dependent transcriptional changes in multiple proinflammatory and profibrotic genes of interest. In particular, transcriptional profiles for *Il1β* (**A**), *Mmp3* (**B**), *Mmp13* (**C**), *F4/80* (**D**), *Cd14* (**E**), *Mrc1* (**F**), *Tgfβ* (**G**), *αsma* (**H**), *Col1a1* (**I**), and *Flk1* (**J**) are shown. * $p < 0.05$ between treatments, # $p < 0.05$ relative to Sham, ^ $p < 0.05$ relative to previous time point.

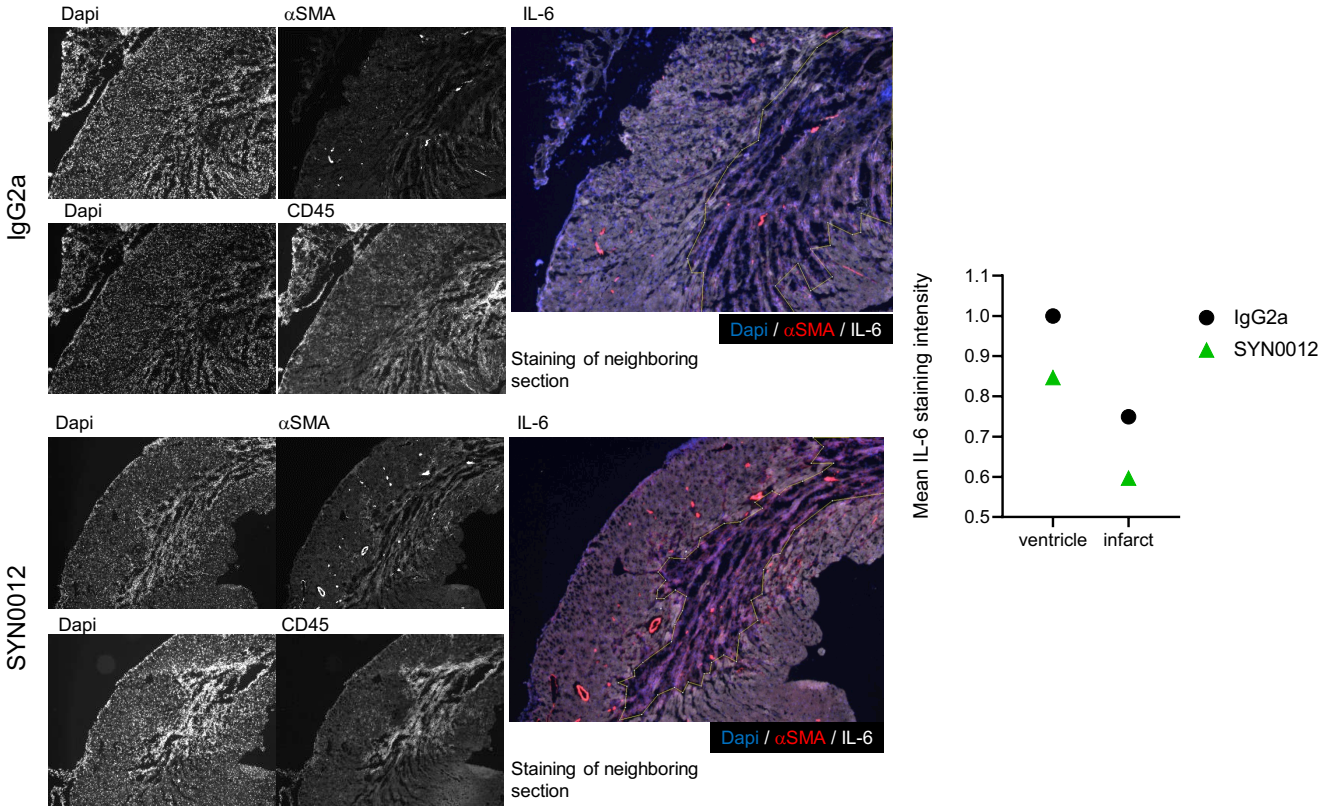

Figure S15: Immunostaining of infarct and peri-infarct regions of IgG2a and SYN0012 treated heart. Neighboring sections were stained with IL-6, aSMA and CD45 antibodies, along with Dapi, to colocalize expression of IL-6 with myofibroblasts and bone-marrow derived cells. The area without CMs was deemed the infarct area (outlined in yellow in the far right panels) and the average IL-6 signal intensity in this region was quantified and compared to the average intensity from the whole area of the ventricular myocardium from these images.

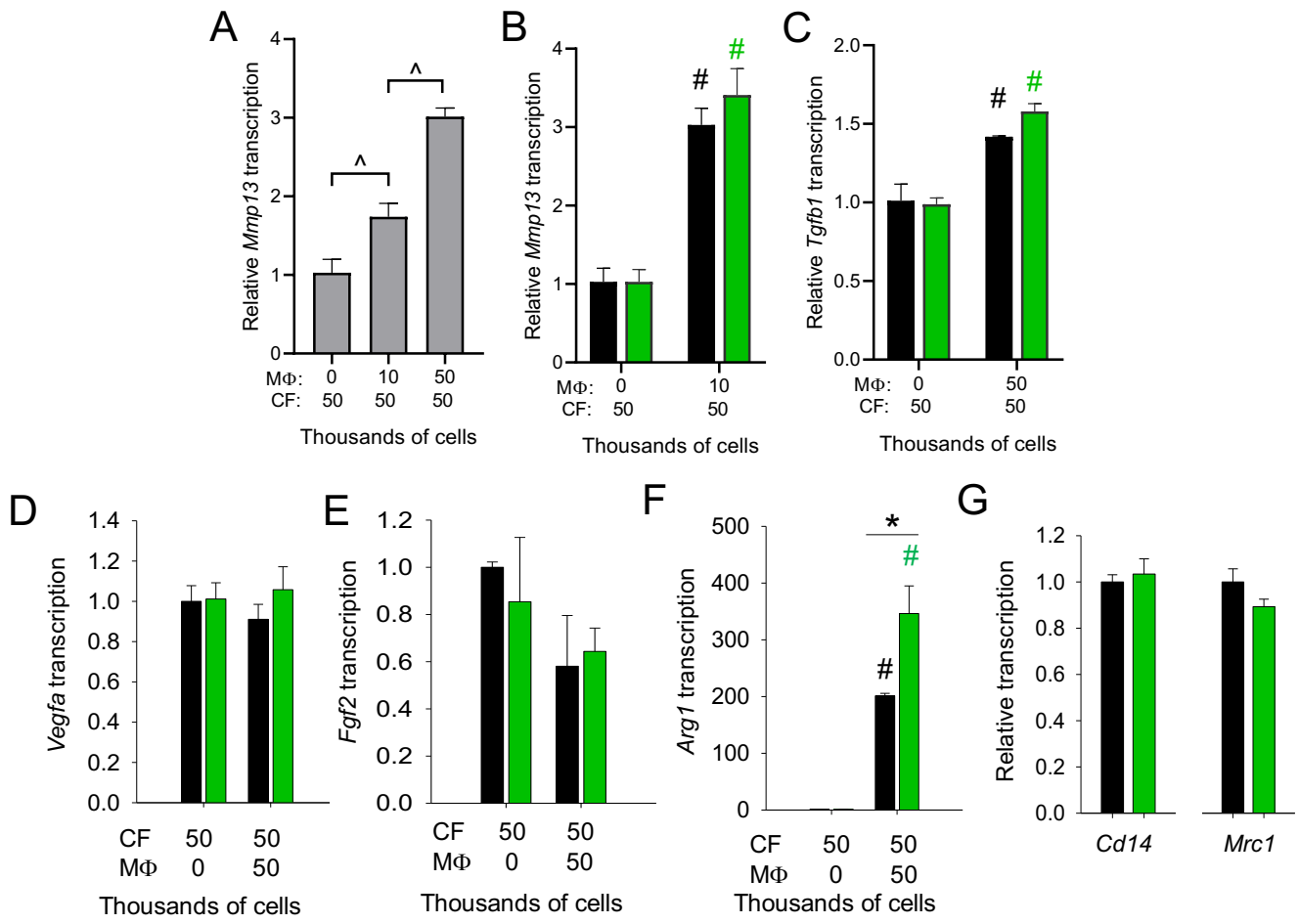

Figure S16: Effect of CF-MΦ co-culture on transcription of profibrotic, proangiogenic, and macrophage polarization markers. *MMP13* transcription was significantly increased with macrophage number (**A**). *MMP13* (**B**) and *Tgfb1* (**C**) transcription both increased with MΦ coculture, but were not significantly altered by SYN0012 treatment. There were no transcriptional differences in proangiogenic growth factors *Vegfa1* (**D**) and *Fgf2* (**E**) with SYN0012 treatment. Additionally, *Vegfa1* transcription was not dependent upon MΦ concentration, whereas *Fgf2* showed a trend toward decreasing transcription with increasing number of MΦs in the co-culture. Conversely, there was a significant increase in *Arg1* transcription – a marker of M2 macrophage polarization – with SYN0012 treatment (**F**), but no difference in M1 and M2 macrophage markers *Cd14* and *Mrc1*, respectively (**G**). * $p > 0.05$ between treatments, # $p > 0.05$ relative to CF-only group; n = 3-4 for all samples.